HIGH-ALPHA VORTEX DECOUPLING INVESTIGATIONS ON A CHINE FOREBODY/DELTA WING CONFIGURATION AT TRANSONIC MACH NUMBERS

Dhanvada M. Rao and M. K. Bhat

VÍGYAN, INC.
Hampton, Virginia

NASA

National Aeronautics and
Space Administration

Langley Research Center
Hampton, Virginia 23665-5225

ERRATA

NASA Contractor Report 189642

High-Alpha Vortex Decoupling Investigations on a Chine
Forebody/Delta Wing Configuration at Transonic Mach Numbers

Dhanvada M. Rao and M. K. Bhat

June 1992

Attached is a corrected copy of NASA Contractor Report 189642. Beginning with page 36, the wrong figures were inadvertently printed in the report which was previously sent to you. Please destroy all copies of the report that you previously received.

HIGH-ALPHA VORTEX DECOUPLING INVESTIGATIONS ON A CHINE FOREBODY/DELTA WING CONFIGURATION AT TRANSONIC MACH NUMBERS

Dhanvada M. Rao and M. K. Bhat

ViGYAN, Inc.

ABSTRACT

This report deals with a test program conducted in the NASA Langley 8-foot Transonic Pressure Tunnel on a blended chine/delta wing model, to verify the concept of controlled vortex decoupling via inboard leading-edge flaps for improved high-alpha lateral/directional characteristics. This test extended the Mach number range of a data base previously generated in a Langley 7-by 10-foot High Speed Tunnel investigation. Six-component force/moment, forebody surface pressures, and central and twin tail static and dynamic loads were measured at Mach numbers of 0.4 to 1.2; laser light-sheet visualizations were also performed. Selected data are analyzed and discussed, emphasizing lateral/directional improvements and tail environment enhancement attainable by leading-edge flaps in the maximum lift region.

SYMBOLS & ABBREVIATIONS

Force and moment data presented in this paper have been reduced to conventional coefficient form based on the wing trapezoidal planform area (extended to the fuselage centerline). Moments are referenced to the balance center. All dimensional values are given in U.S. Customary Units. The symbols are defined as follows:

b	wing span, 19.20 in		S	wing planform reference area, 208.224 in^2
b_f	LEF span, in.			
C_L	lift coefficient, Lift/qS		Y	spanwise distance from model centerline, in.
$C_{L,MAX}$	maximum lift coefficient			
C_l	rolling moment coefficient, Rolling moment/qSb		α	angle of attack, deg.
C_m	pitching moment coefficient, Pitching moment/qSc		β	angle of sideslip, deg.
C_n	yawing moment coefficient, Yawing moment/qSb		C.V.T.	central vertical tail
C_p	pressure coefficient		LEF	leading edge flap
c	mean geometric chord of reference wing panel, 10.92in		V.T.	vertical tail
M_∞	free-stream Mach number		T.T.	twin tail
q	free-stream dynamic pressure,psi			
Re	Reynold number		RMS	root mean square of tail gage voltage output
SF	side force, lb			

INTRODUCTION

The beneficial interaction of forebody chine vortices with the leading-edge separated flow-field of highly swept delta wings is known to significantly improve the maneuvering lift capability of such configurations in the moderate to high alpha range. When the coupled chine-wing vortices eventually break down, however, severe stability and handling difficulties arise particularly in the presence of sideslip. In order to alleviate these problematical near-stall and post-stall aerodynamics, a concept of controlled decoupling of chine and wing vortices was proposed and subjected to an exploratory low-speed tunnel investigation (ref.1). The results of that precursor study demonstrated the feasibility of artificially maintaining a decoupled vortex system up to high angles of attack and sideslip on a generic, close- coupled chine delta configuration of simplified geometry. Inboard leading-edge flaps were found to be particularly effective in vortex decoupling, and resulted in beneficial post-stall characteristics, viz., pitch down and lateral/directional stability in the $C_{L, MAX}$ region.

The second study (ref. 2) dealt with tests at low subsonic Mach numbers (0.1 and 0.4) in the Langley 7-by 10-Foot High Speed Tunnel (HST), employing a more realistic model geometry (viz., blended chines and airfoil wing sections). This test generated an extensive data base comprising six-component force/moment coefficients, forebody and wing surface pressure and laser light-sheet flow visualizations. Its results generally corroborated the aerodynamic trends of the preliminary exploration of controlled vortex decoupling benefits at high angles of attack.

In this report, results are presented of a test entry in the Langley 8-Foot Transonic Pressure Tunnel (TPT) performed to extend the data base on the ref. 2 model to higher Mach numbers. This report includes a discussion of vertical tail static and dynamic characteristics, Mach number effects on the force/moment and chine suction pressure characteristics, and presents laser-sheet visualizations.

FACILITY, EQUIPMENT, MODEL AND TEST PLAN

The Langley 8-Foot TPT is a closed-return, variable pressure/temperature facility, with a continuous Mach number capability up to 1.2 (see ref. 3). The model was supported on a sting incorporating a yaw coupler allowing combinations of α and β in the ranges 7° to 32° and $\pm$ 7°, respectively. The facility is equipped with a laser light-sheet illumination system. In order to obtain natural condensation over the model, water is injected into the tunnel circuit just aft of the test section. The flow pattern was monitored and recorded with a video camera located on the sting.

The blended chine forebody/delta wing test model is shown in fig. 1. This was the same model as tested in the 7- by 10-Foot HST and described in ref.2. The model is equipped with full span leading-edge flaps divided into three equal span segment, the inner two segments being deflectable at 0, 10, 20 or 30 deg. on independent brackets. For the current test involving considerably higher free-stream dynamic pressures, the electronically scanned pressure (ESP) modules located external to the model in ref. 2 were deleted leaving the three forebody stations and only a part of the first wing station available for pressure measurements with onboard ESP modules. A photograph of the model installation is presented in fig. 2.

The test plan comprising the model configuration and Mach number is summarized in Table I. The corresponding values of Re_c for M_∞ = 0.4, 0.6, 0.7, 0.8, 0.9 and 1.2 were, respectively, 2.1, 2.0, 2.0, 2.0, 1.9 and 1.6 million.

RESULTS AND DISCUSSION

Flow Visualization

Still photographs extracted from a rather extensive vapor-screen video recording of this test are presented in figs. 3 through 12. This selection includes the tail-off, central tail and twin-tail configurations with and without leading-edge flap deflection, at α = 20° and 26°, and at $\beta \geq 0°$, at a constant Mach number of 0.9 while allowed the vortex patterns and shocks to be observed. Note, however, that lack of humidity control resulted in varying levels of vapor condensation from one test to another, which could affect the interpretation of these visualizations.

i) Tail off; 0° LEF: As shown in fig. 3, the leeside flow at α = 20° is dominated by chine vortices, with incipient or weak leading edge separation. An asymmetry in the chine vortices probably indicates a small degree of positive sideslip. At α = 26°, a unique flow structure appears across the wing span, consisting of multiple vortices arranged outboard of the chine vortices. From the symmetry and regular spacing of these wing vortices, they are suspected to originate from minor gaps present at the flap segment joints. A bright envelop covering the vortex systems on either side may be associated with increasing droplet concentration due to a funneling of the flow into a narrow central region by the intense downwash induced between the vortices. Also seen at α = 26° is a shock pair above the vortical envelops; these are believed to constitute the cross-flow shocks (e.g. ref.4) which return the leeside

streamlines, deflected inwardly during their expansion over the wing, to a direction parallel to the symmetry plane. Miller and Wood in ref. 4 have proposed an extended chart based on the components of Mach number and angle of attack in the plane normal to the leading edge, which delineate various leeside flow regimes experimentally observed on planar delta wing (fig. 4). Neglecting the influence of the chine forebody of the present configuration, this chart predicts the 60° delta wing to generate these cross-flow shocks at $\alpha = 26°$ but not at $\alpha = 20°$ corroborating the present visualization results.

ii) <u>Tail Off: 2/3-Span 30° LEF</u>:   Fig. 5 shows the chine vortices becoming more prominent as the leading-edge vortices are suppressed by flap deflection. The cross-flow shocks are not in evidence at $\alpha = 26°$, which could be due to a diminished expansion over the cambered leading edges, or reduced condensation, or a combination of the two effects.

iii) <u>Central Tail: 0° LEF</u>:   The flow patterns remain essentially unchanged by the addition of the central tail (compare fig. 6 with fig. 4). The cross-flow shocks are better defined however, probably as a result of more favorable condensation environment attained during these test runs.

iv)   <u>Central Tail: 2/3-Span 30° LEF</u>:   The $\alpha = 26°$ case (fig. 7) particularly well depicts the decoupled chine and wing vortices. Also, the lambda-shaped shock structures overlying the vortical regions are clearly seen, which again may indicate a more favorable state of condensation obtaining during this test (in contrast to the tail-off case, see (ii) above).

v) Central Tail; 0° LEF; Sideslip: At ß = 3° (fig. 8) the windward wing panel shows a greatly expanded vortical region suggestive of vortex merger and breakdown, whereas the leeside chine vortex shrinks in size and is also elevated (compare with ß = 0° case in fig. 6). The downwash 'funnel' has moved off the symmetry plane to the left half of the fuselage, and the expanded right-wing vortical zone is influencing the tail. With increasing sideslip the leeward chine vortex continues to diminish, and appears to have decoupled at ß = 6°.

vi) Central Tail; 2/3-Span 30° LEF; ß>0°:   Flap deflection allows the windward chine vortex to remain as a coherent structure at ß = 3°, decoupled from the wing flow (fig. 9). On the leeside, a second smaller vortex-like feature appears close to the chine vortex, which is tentatively identified as the vortex starting from the undeflected outboard flap segment (also visible, less definitively, in fig. 8). Increasing sideslip shows the windward chine vortex to migrate inboard, crossing the tail at ß = 6°.

vii) Twin Tails; With and Without Flaps: Visualizations at α = 26°, ß = 0° with and without flap deflection are presented in fig. 10. The chine vortices remain well inboard of the tails, their position and appearance not visibly affected by flap deflection. The main effect of 2/3-span flaps is the formation of wing vortices over the outboard undeflected leading edges which apparently do not interact with the chine vortices.

viii)   <u>Twin Tails; 0° LEF; ß > 0°</u>:   The effect of sideslip (fig. 11) is essentially similar

to that previously described for the central-tail case, viz., an expanded vortical region on the

windward panel while the leeward chine vortex tends to shrink in size.   Although the

leeward vortex moves closer to the corresponding tail with increasing sideslip, it remains

coherent showing no sign of breakdown from tail impingement.

ix)   <u>Twin Tails; 2/3-Span 30° LEF; ß > 0°</u>:   In this case (fig. 12) the windward chine

vortex apparently is generally unaffected by the wing separation (in contrast to the central

tail case, fig. 9) with only its trajectory being displaced inward by the positive sideslip. From

photographs not shown, a co-rotating vortex formed at the tail leading edge on the windward

side appears to feed the adjacent chine vortex and may contribute to its stability at the

higher side-slip angles.

Force/Moment Characteristics at Zero Side-Slip

The ß = 0° lift and moment coefficients with increasing angle of attack, showing the

effects of Mach number on the various model configurations, are presented in figs. 13

through 21.   In the first set of data plots pertaining to the tail-off and flap zero case (fig.

13), increasing Mach number is generally seen to cause a lift deterioration at angles of

attack above 20°, and a negative pitching-moment increment due to aft movement of the

center of pressure. These Mach number trends are only mildly affected by leading-edge flap

deflection (figs. 14 and 15).   Addition of the central tail (figs. 16 to 18) also does not

noticeably change these ß = 0° characteristics. The twin-tail case (figs. 19 to 21) on the other

7

hand, produces distinctively adverse longitudinal aerodynamic effects. A marked deterioration of lift is seen above α = 15° at all the subsonic Mach numbers, together with a pronounced pitching moment increment which indicates the lift loss to mainly occur over the aft region of the wing, i.e., in the vicinity of the twin tails. This adverse twin-tail effect has already been demonstrated in the wing pressure measurements reported in ref. 2.

A comparison of the ß = 0° lift and moment data, between the present 8-Foot TPT results and those obtained in the 7- by 10-Foot HST test (ref. 2) for a typical case (i.e., central-tail configuration) at a common Mach number of 0.4 is presented in figs. 22 to 24. While support limitations precluded the attainment of stall angle of attack in the 8-Foot TPT tests, the data comparison between the two facilities shows excellent agreement. A typical comparison of the forebody pressure data at a nominal α = 30° presented in fig. 25 is also seen to be quite satisfactory.

Lateral/Directional Stability Characteristics:

The rolling- and yawing-moment characteristics of the central tail configuration will first be discussed, using the beta-sweep results at a nominal 30° angle of attack (which for the 7- by 10-Foot HST data is about 7° below the angle of attack for $C_{L,MAX}$ for most configurations). Rolling-moment coefficient versus beta for four Mach numbers are presented in fig. 26. Data for α = 30° and M_∞ = 0.9 could not be taken in the 8-Foot TPT due to tunnel blockage restrictions (data at α = 26° has been substituted). In the 0° LEF case, M_∞ = 0.4 and 0.7 data reveal pronounced discontinuities and reversals of the rolling moment

8

with relatively small beta increments, which highlight the extreme lateral sensitivity of the baseline configuration when approaching $C_{L,MAX}$. The 1/3-span and 2/3-span leading-edge flaps alleviate the severity of these reversals and/or extend the beta range lateral stability at all Mach numbers. The corresponding directional characteristics are presented in fig. 27. The M_∞ = 0.4 and 0.7 data clearly indicate improvements due to the flaps at the higher sideslip angles where a reduction of directional stability was seen in the 0° LEF case. Although the asymmetry on either side of ß = 0° of these data partially mask the comparative effectiveness of 1/3-span and 2/3-span flaps, trends in the ß > 0° range indicate that the benefits are in proportion to the flap span. This would imply that vortex decoupling as well as wing flow improvement may equally be responsible, whereas the 7- by 10-Foot HST results (ref. 2) indicated a preeminence of decoupling effect due to the inboard 1/3-span flaps.

A comparison of the lateral/directional characteristics at M_∞ = 0.4 measured in the two facilities is presented in fig. 28. The rolling moment coefficient versus beta for the nominal α = 30° case show opposite trends within the narrow ß = ± 3° range, which may partly be related to a 4.3° difference between the actual angles of attack for the two data sets. A positive conclusion from this comparison is that the results from both facilities are in agreement regarding the extreme high-alpha lateral sensitivity of the test configuration.

Next, the twin-tail configuration is considered in comparison with the central tail. As shown in figs. 29 and 30, even with the flaps undeflected the twin-tail case at all Mach

numbers is stable both laterally and directionally at the small sideslip angles, and also relatively free of the severe moment reversals observed with the central tail. The benefit of flap deflection is seen mainly at higher sideslip angles where the 0° LEF twin-tail configuration reaches a lateral stability limit, indicated by the M_∞ = 0.4 and 0.7 data (fig. 31). The twin tails inherently are highly stable directionally at all Mach numbers and the effect of flap deflection is negligible (fig. 32).

Tail Load Characteristics

i) Central Tail: The average steady and fluctuating tail load characteristics versus sideslip angle, showing the effects of leading-edge flaps and Mach number, are presented in figs. 33 to 35 for a nominal α = 30°. Note that the steady tail 'side force' is based on a calibration of the tail root strain output against a normal load applied at the tail centroid, positive force being to the 'pilot's' right; the fluctuating load is expressed as RMS of the tail-gage output voltage.

The steady tail load is seen to vary linearly with sideslip angle, up to ß = ± 2.5° with undeflected flaps through the Mach number range. At this sideslip angle a 'tail-stall' is indicated, which on the basis of flow visualizations (see fig. 8) is apparently triggered by the windward vortical region enveloping most of the tail height. With the 1/3-span and 2/3-span flaps at 30° deflection, the tail 'stall' onset is moved up to ß = ± 5° with the 2/3-span flaps producing a somewhat less abrupt loss of the tail load after stall than the 1/3-span flaps.

10

The fluctuating tail load RMS characteristics, presented directly below the steady-load data plots in figs. 33 to 35, show a dramatic increase in tail excitation at a sideslip angle coinciding with the steady-load stall. Equally remarkable are the progressive improvements in the dynamic output achieved with 1/3-span and 2/3-span leading-edge flaps. These results can be understood with reference to the flow visualizations of fig. 9, where flap deflection is seen not only to diminish the windward stall region but, more importantly for alleviation of tail excitation, to vortically restructure the separated flow thus presumably stabilizing it and reducing its dynamic content.

ii) Twin Tails: At high angles of attack the wing-mounted tails were expected to encounter an intensively dynamic environment due to wing separations, vortex interactions and breakdown. The character of RMS output of tail gages confirmed this expectation; indeed the noise content of the outputs was too high to allow a meaningful analysis. However, the averaged signals provided useful information on the steady tail load characteristics with respect to flap deflection and Mach number effects, as discussed below.

Results of beta-sweep tests at nominal α = 20° and 30° and various Mach numbers are shown in figs. 36 to 39. The averaged side force on left and right tails is separately plotted versus sideslip angle, with and without flap deflection. In the zero flap case at ß > 0°, the (windward) right tail generates a negative (i.e. stabilizing) side force (SF) whereas the left tail is practically ineffective. On the evidence of flow visualizations (fig. 11), this behavior may be explained as follows: at ß = 0° the induced suction of the chine vortices

11

passing in-between the twin tails generates equal and opposite tail forces (i.e., negative SF on the right tail and positive SF on the left tail, as shown by the 0° LEF data at α = 20° in fig. 36). At positive sideslip angles, the left chine vortex moves closer to the left-tail inner surface thus increasing its suction-induced positive side force, which opposes the effect of positive sideslip and thus degrades the left-tail effectiveness. On the other hand, the remaining vortex suction effect over the right-tail inner surface reinforces its negative side force produced by sideslip. With flap deflection, chine vortex suction appears to assume lesser importance (as indicated by the ß = 0° side force data at α = 20°), the primary driver being the improved wing flow allowing the twin tails to operate at increased local dynamic local pressure. These flap-generated improvements in the twin-tail side force characteristics become more pronounced with increasing Mach number. As shown by the M_∞ = 0.9 data at α = 20° (fig. 38) with 1/3-span flap deflection the tail side force is rendered practically linear in the range - 4°< ß < 4°, with the tails becoming equally effective both in positive and negative sideslip. Here, a further improvement shown by 2/3-span over the 1/3-span flap is evidently a result of additional wing flow clean-up.

CONCLUSIONS

A follow-up investigation was conducted in the NASA Langley 8-Foot Transonic Pressure Tunnel in order to extend the data base, generated during a preceding test entry in the Langley 7- by 10-Foot High Speed Tunnel on a blended chine forebody/delta wing/leading-edge flap model, to high subsonic/ transonic Mach numbers. The main results of this test may be summarized as follows:

1. Data comparisons between the two facilities showed excellent agreement in the ß = 0° force/moment and forebody suction pressure characteristics. Certain differences in detail were noted in the high-alpha lateral behavior within a narrow range of sideslip angle; nevertheless, the data generally confirmed the extreme lateral sensitivity of the basic test configuration to rather small beta angles (viz., less than ± 3°) at angles of attack approaching $C_{L,MAX}$.

2. The leading-edge flap benefits to high-alpha lateral/directional stability of the central tail configuration were verified at Mach numbers up to 0.7; at higher M_∞ the flap effects were found to be relatively minor.

3. Central-tail load data confirmed directional effectiveness improvements due to leading-edge flaps at high alpha, and showed dramatic reductions in RMS level implying potential for alleviation of tail buffet. Vapor-screen visualizations indicated these benefits to be associated with vortex decoupling as well as flow improvement on the windward wing panel caused by flap deflection.

4. The twin-tail arrangement produced a radically different high-alpha flowfield devoid of adverse vortex interactions, resulting in highly stable lateral/directional characteristics near stall throughout the Mach number range, albeit with substantial lift penalties. The leading-edge flaps in this case were mainly useful for improving the directional effectiveness at large sideslip angles.

ACKNOWLEDGEMENTS

REFERENCES

1. Rao, D.M., and Bhat, M.K.: "A Low-Speed Wind Tunnel Study of Vortex Interaction Control Techniques on a Chine-Forebody/Delta Wing Configuration". NASA CR-189616, 1992.

2. Rao, D.M., and Bhat, M.K.: "Subsonic Investigations of Vortex Interaction Control for Enhanced High-Alpha Aerodynamics of a Chine Forebody/Delta Wing Configuration". NASA CR-189641, 1992.

3. NASA: " Aeronautical Facilities Catalogue". NASA RP-1132, Vol. 1, page 155, January 1985.

4. Miller, D. S., and Wood, R. M.: "Lee-Side Flow Over Delta Wings at Supersonic Speeds", NASA TP 2430, June 1985.

TABLE 1

Test Model Configurations and Mach Numbers

Case	Vert. Tail			0° LEF	30° LEF Span		Mach Number					
	Off	CVT	TT		1/3	2/3	0.4	0.6	0.7	0.8	0.9	1.2
1	X			X			X		X		X	X
2	X				X		X		X		X	X
3	X					X	X		X		X	X
4		X		X			X		X		X	X
5		X			X		X		X		X	X
6		X				X	X		X		X	X
7			X	X			X	X	X	X	X	X
8			X		X		X	X	X	X	X	X
9			X			X	X	X	X	X	X	X
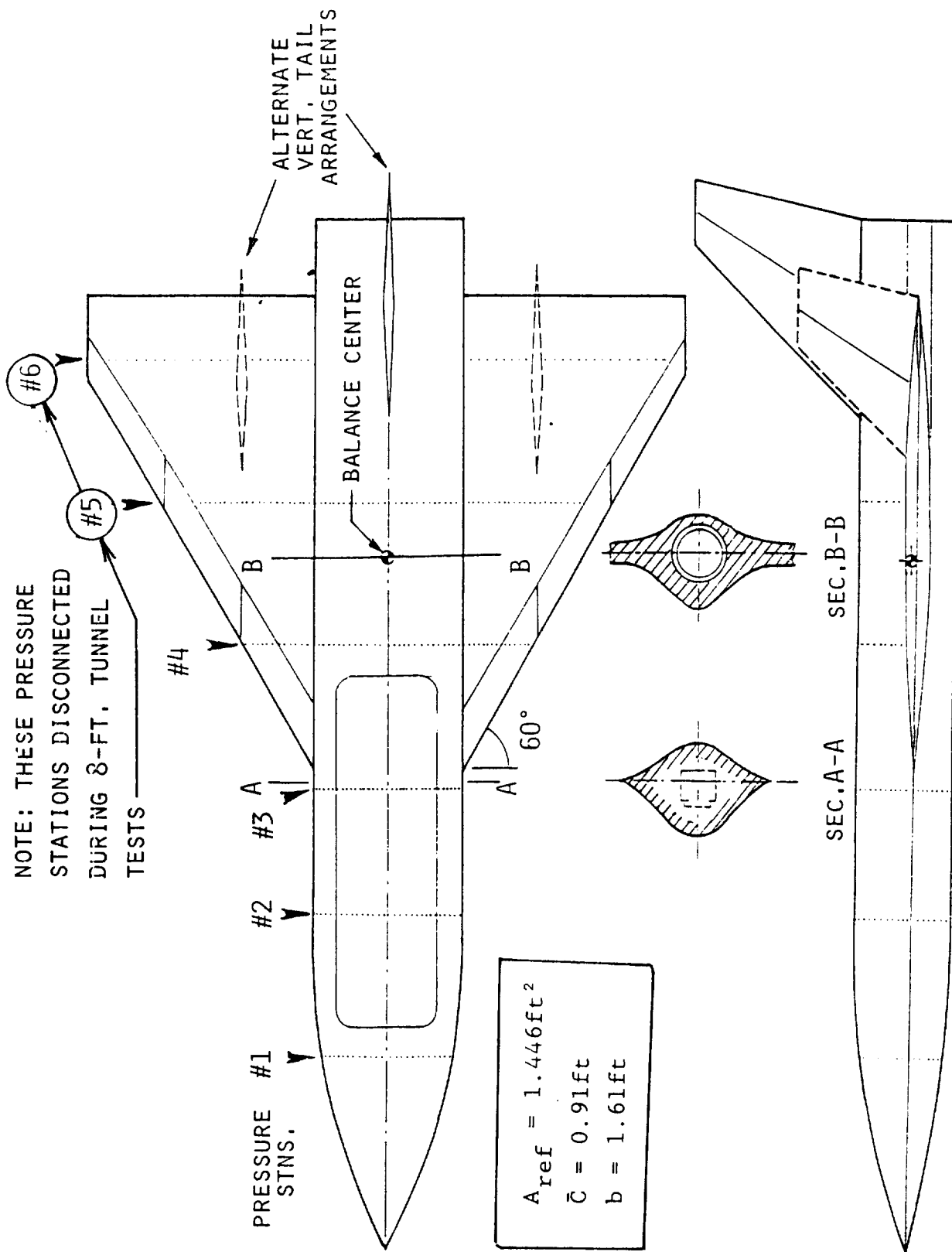
Fig. 1   Test model geometry
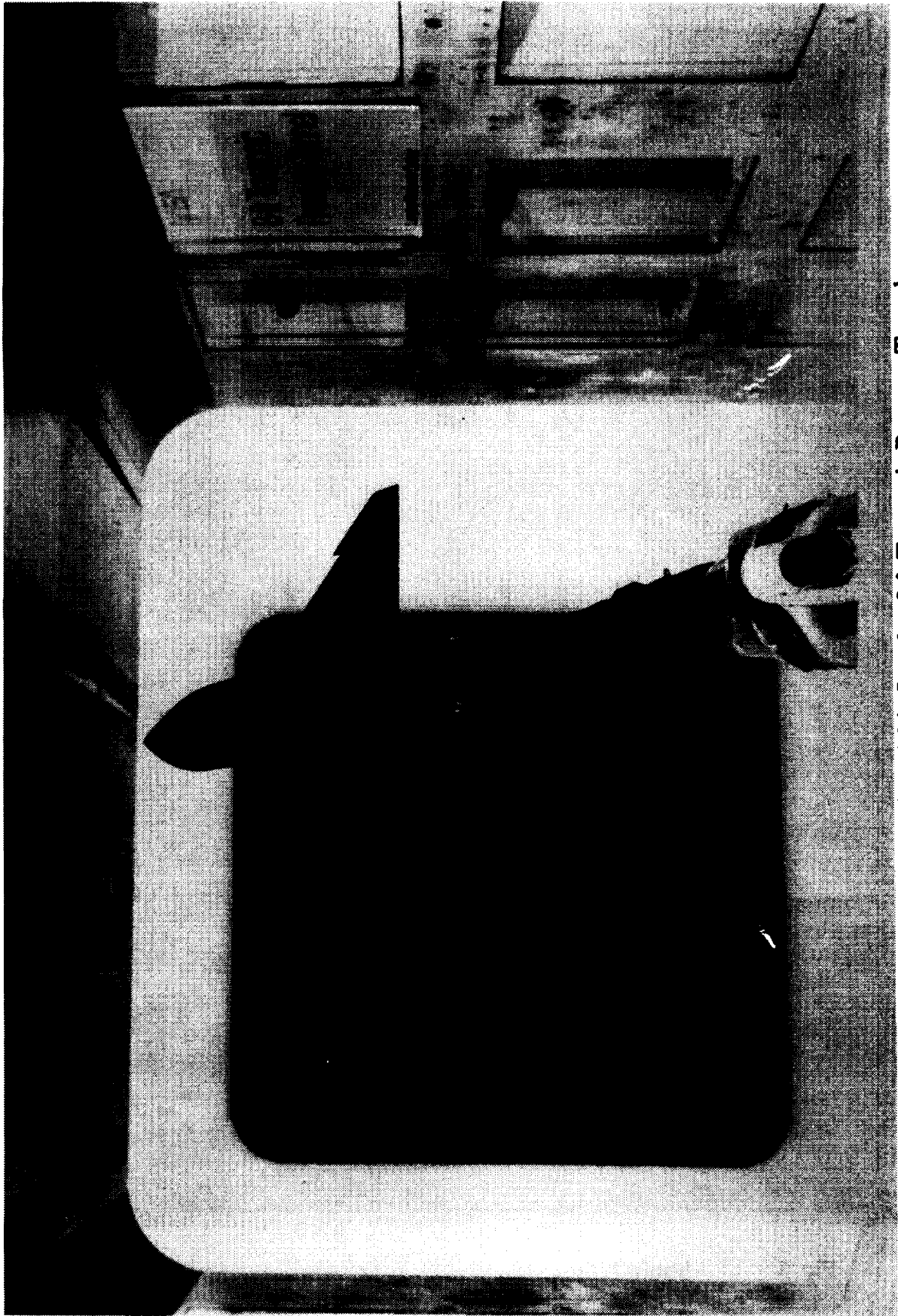
Fig. 2   Photograph of model in Langley 8-ft Transonic Pressure Tunnel.
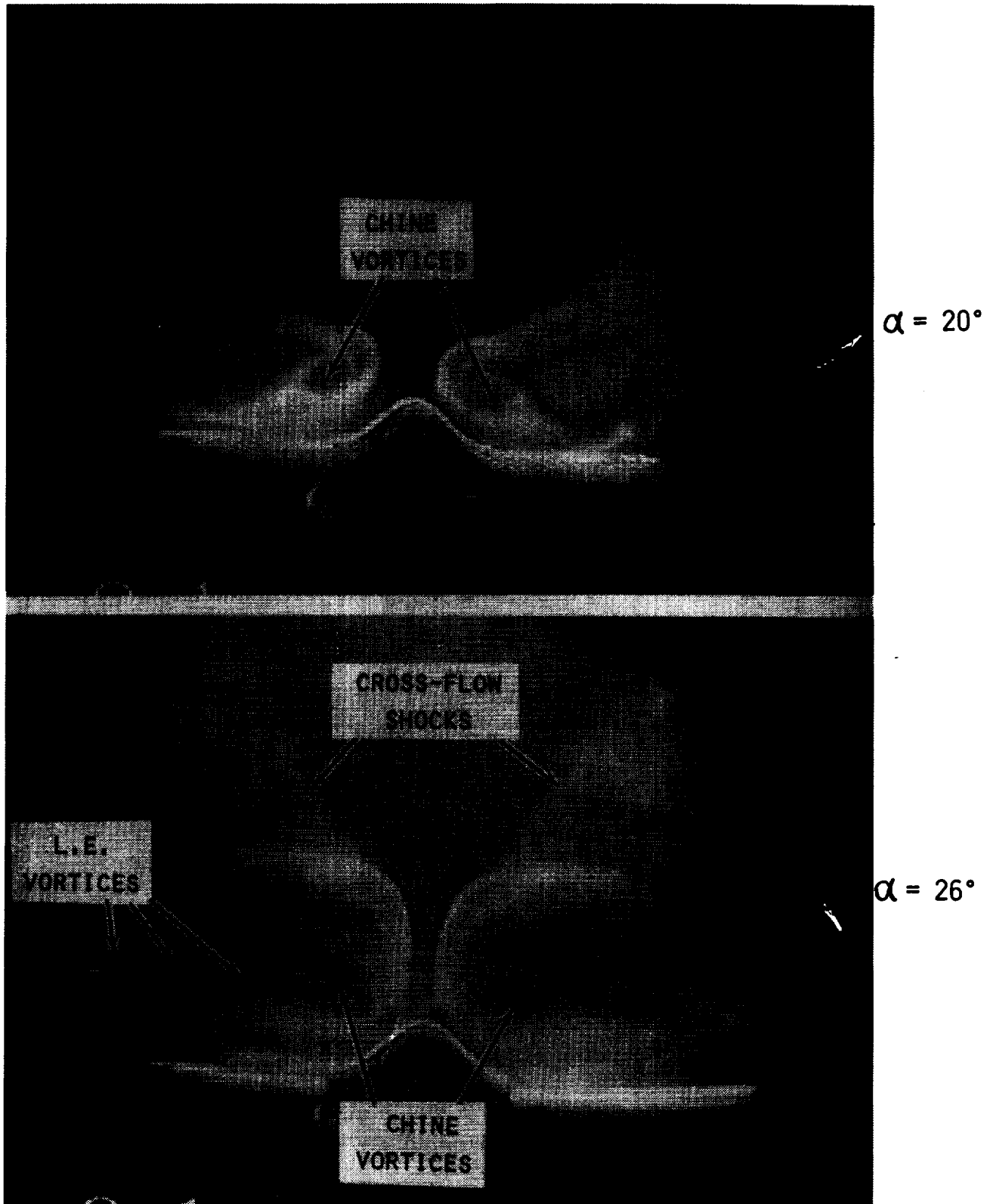
Fig. 3   Vapor screen visualization at M_∞ = 0.9; tail-off configuration; 0° LEF.
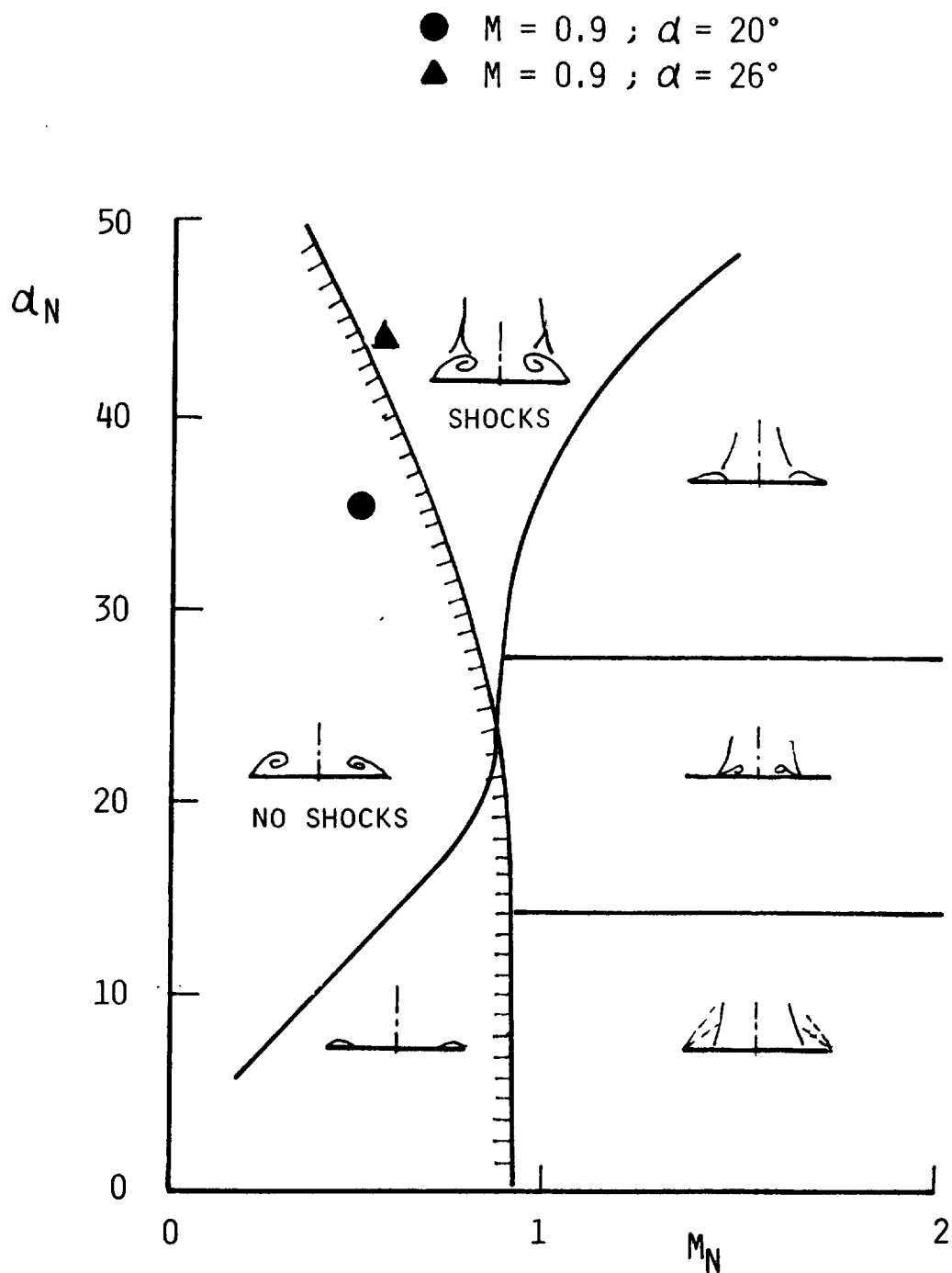
Fig. 4   Assessment of flow visualization results against delta wing lee-side flow boundaries due to Miller and Wood (ref. 4).
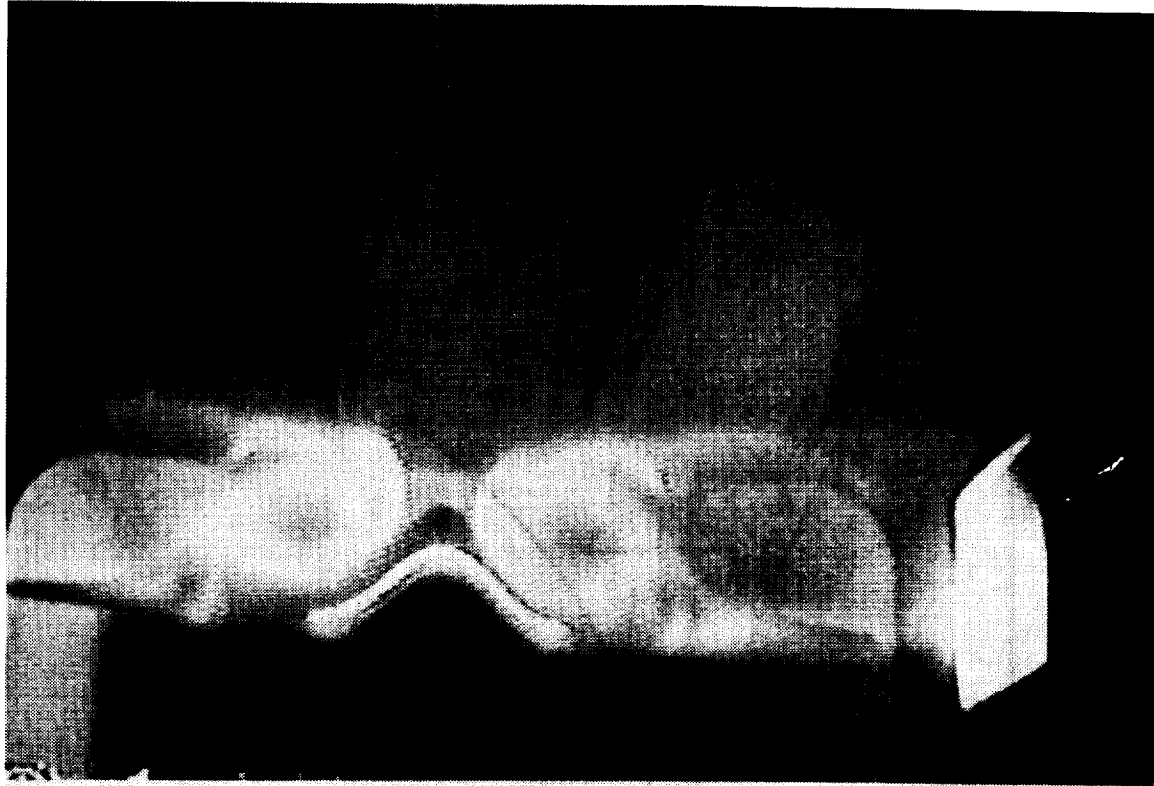
$\alpha = 20°$
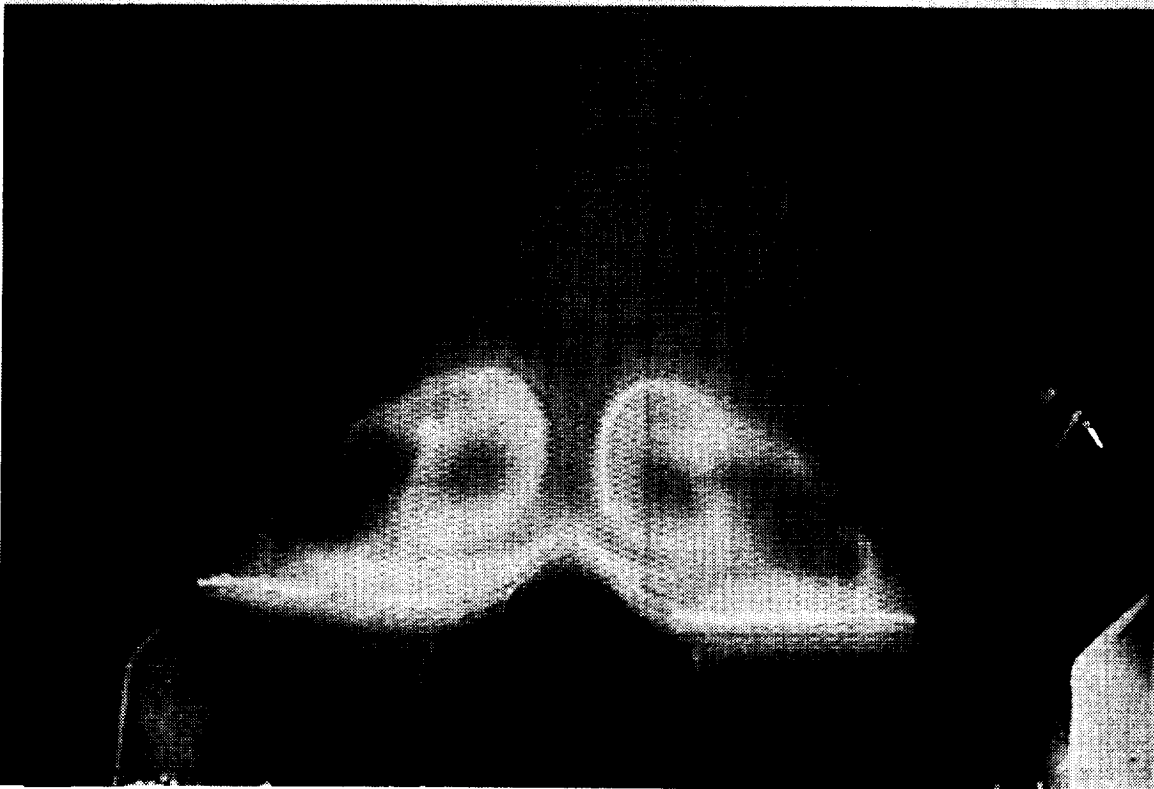
$\alpha = 26°$

Fig. 5   Vapor-screen visualization at $M_\infty = 0.9$; tail-off configuration;
2/3-span 30° LEF.

20

$\alpha = 20°$

$\alpha = 26°$

CROSS-FLOW
SHOCKS

CHINE
VORTICES
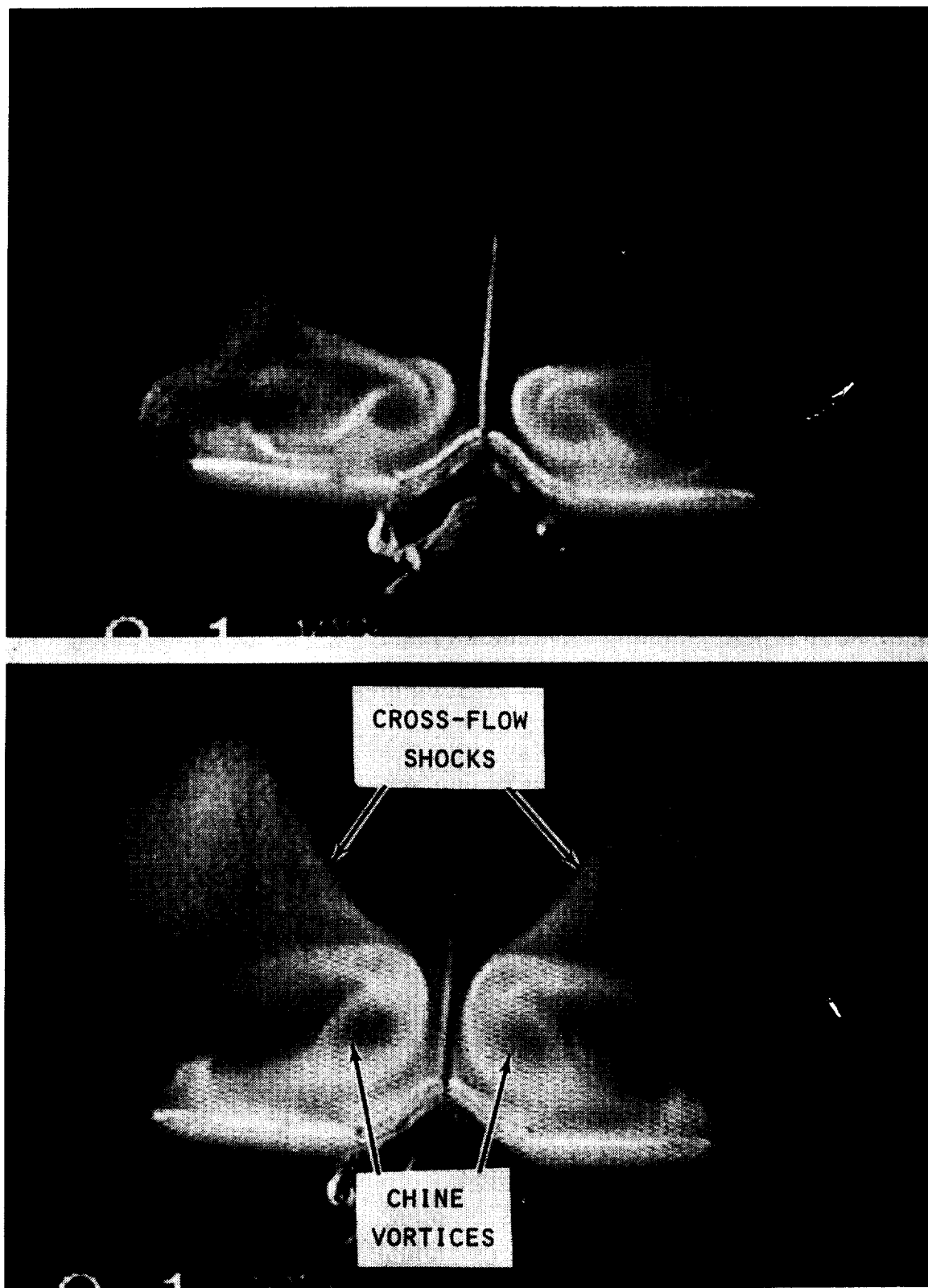
Fig. 6   Vapor-screen visualization at $M_\infty = 0.9$; central-tail configuration; 0° LEF.

21
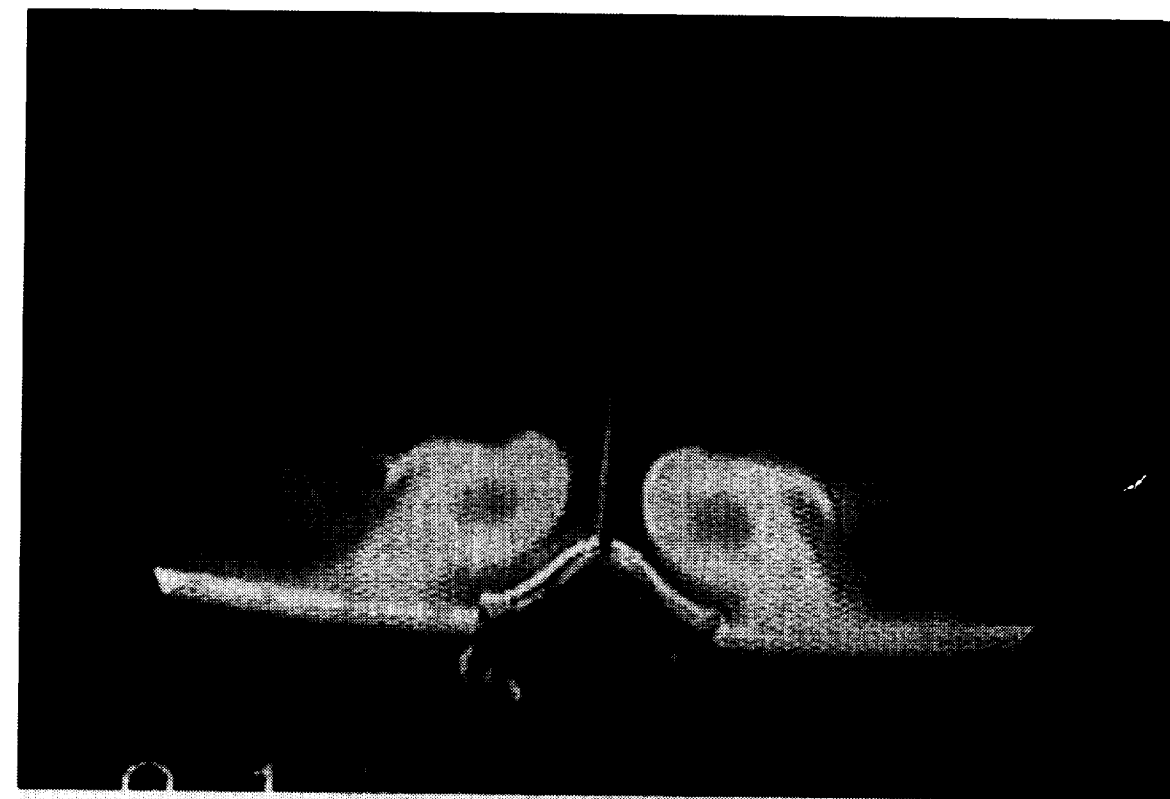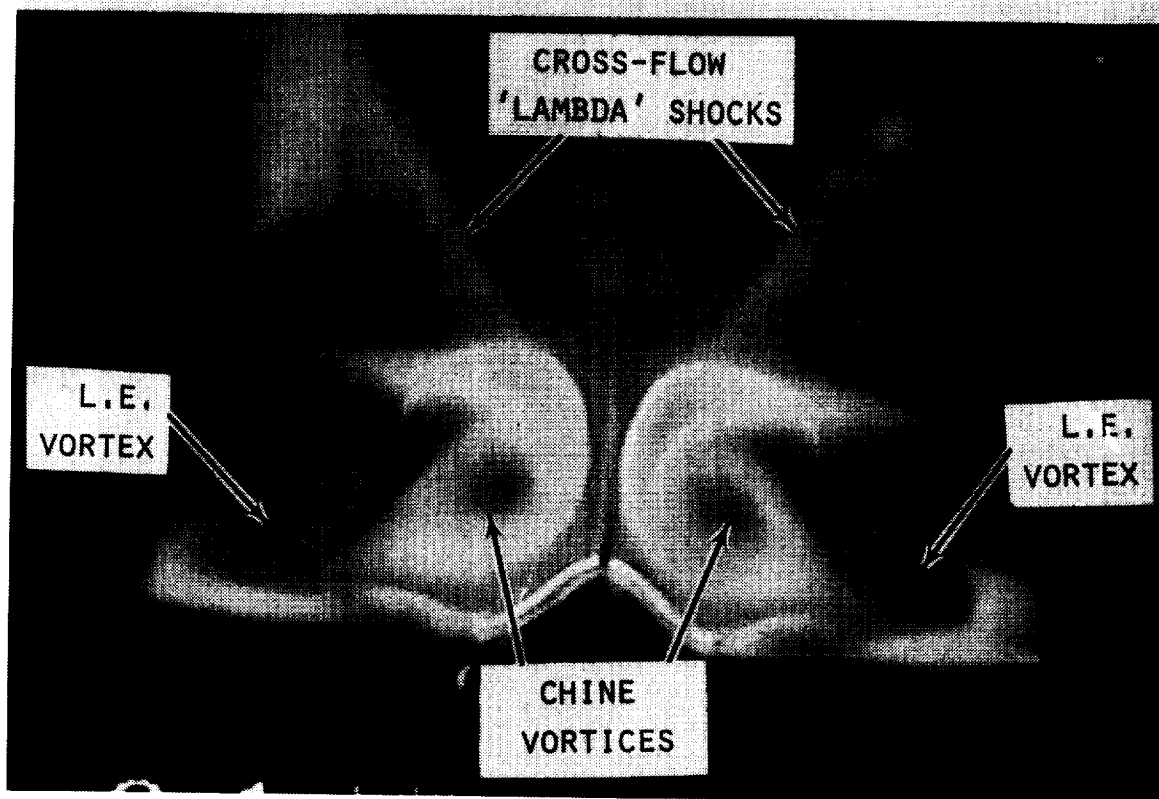
Fig. 7   Vapor screen visualization at $M_\infty = 0.9$; central-tail configuration; 2/3-span 30° LEF.

$\beta = 3°$

$\beta = 4.5°$

$\beta = 6°$
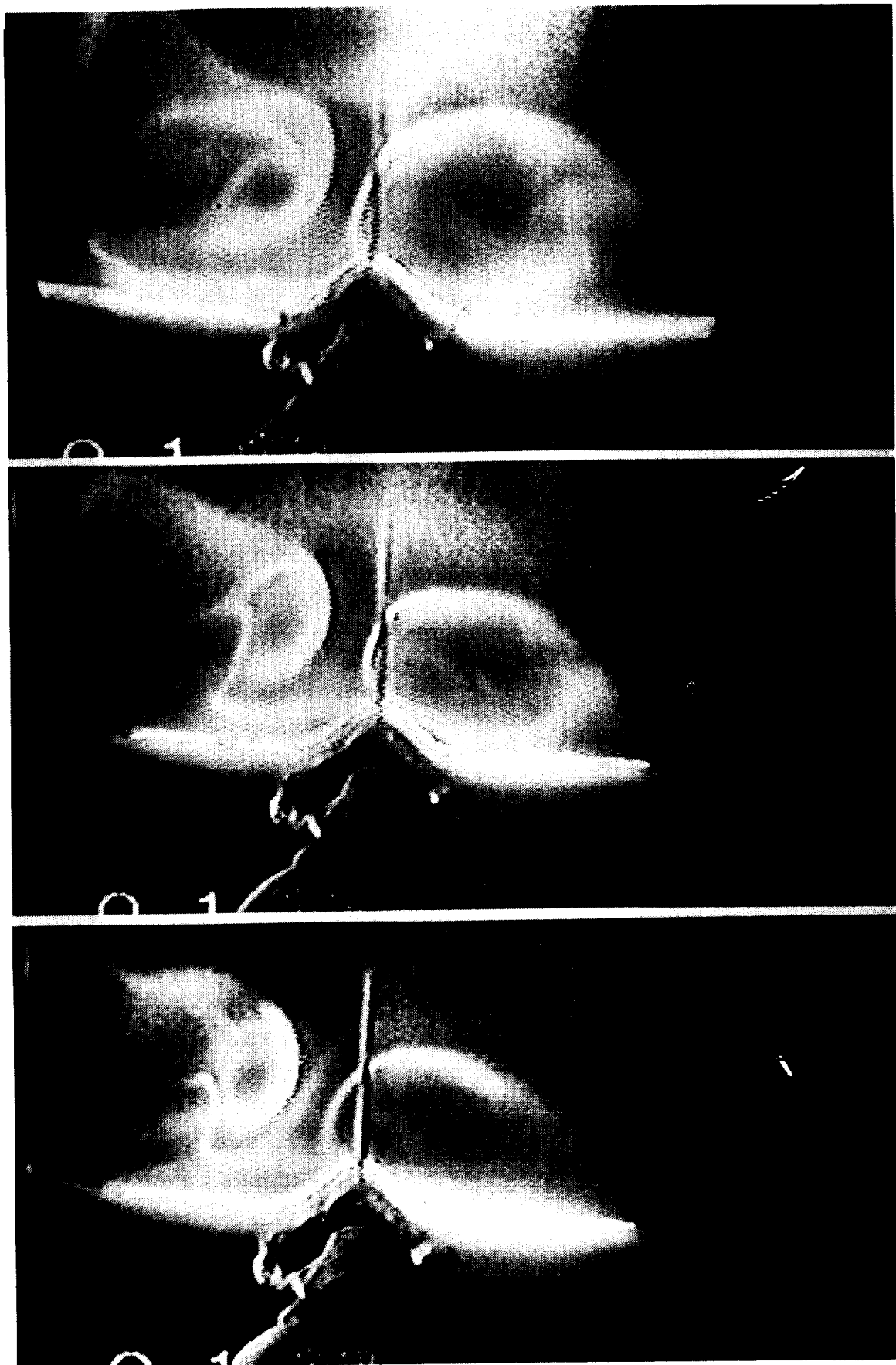
Fig. 8   Vapor screen visualization at $M_\infty = 0.9$; central-tail configuration in sideslip at $\alpha = 26°$; 0° LEF.

23
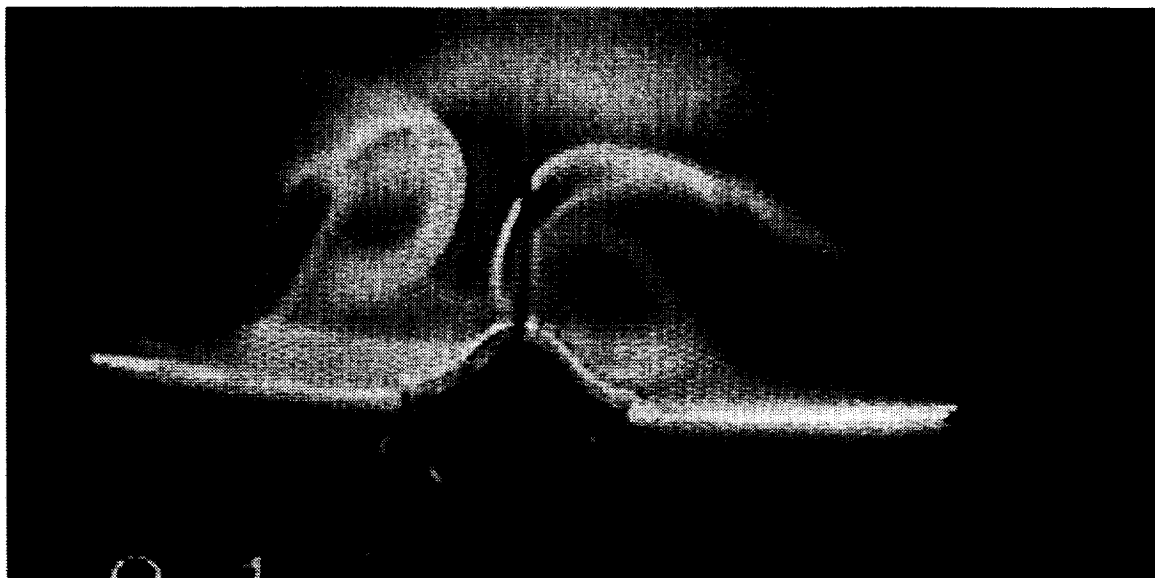
$\beta = 3°$
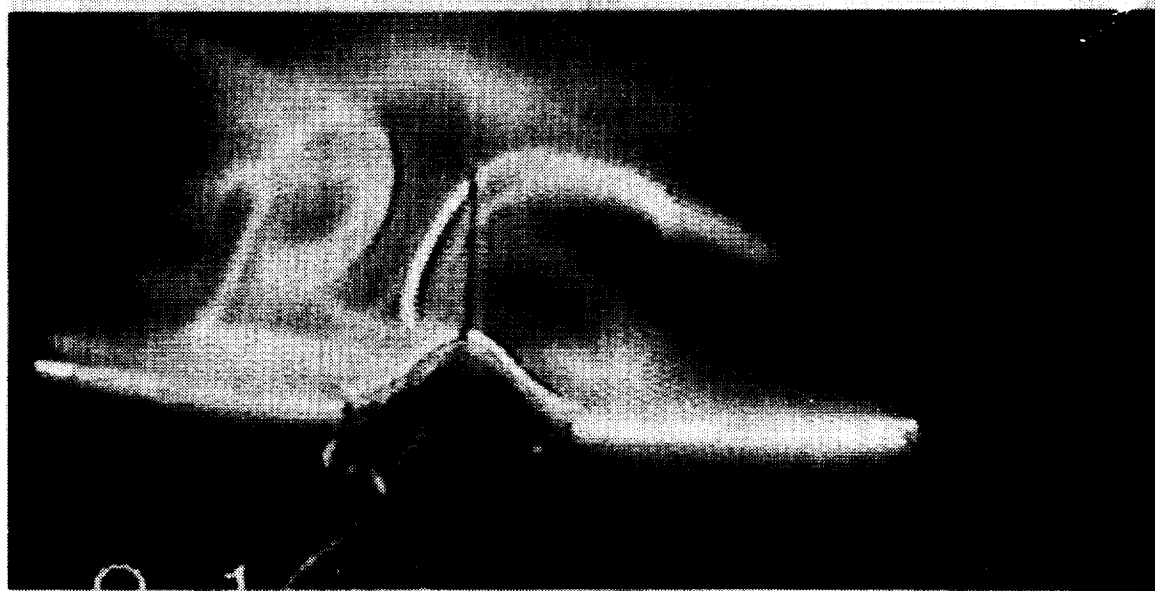
$\beta = 4.5°$
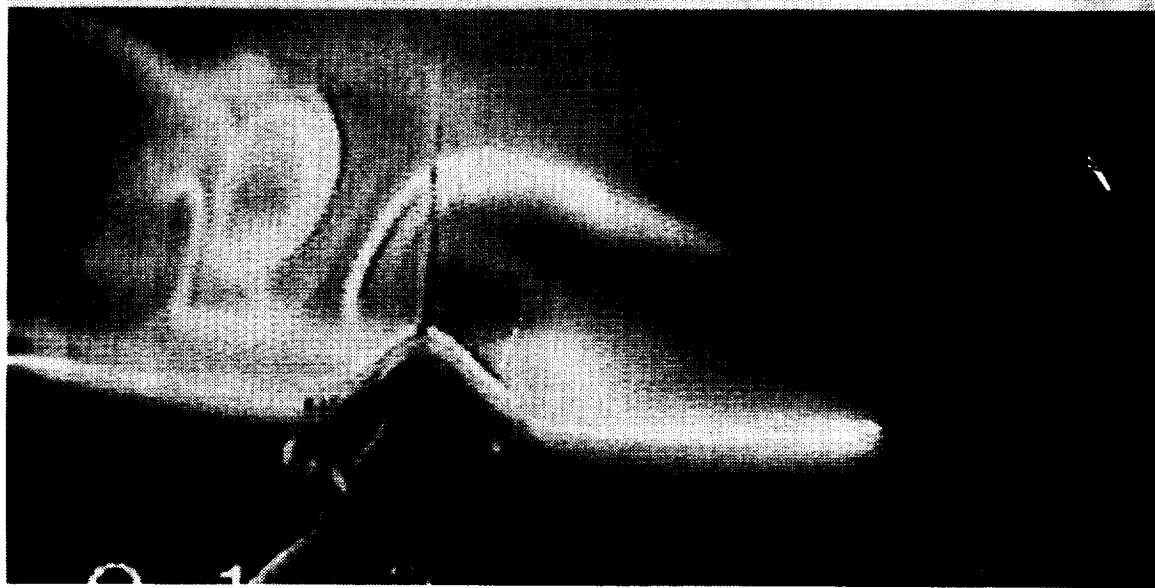
$\beta = 6°$

Fig. 9   Vapor screen visualization at $M_\infty = 0.9$; central-tail configuration in sideslip at $\alpha = 26°$; 2/3-span 30° LEF.
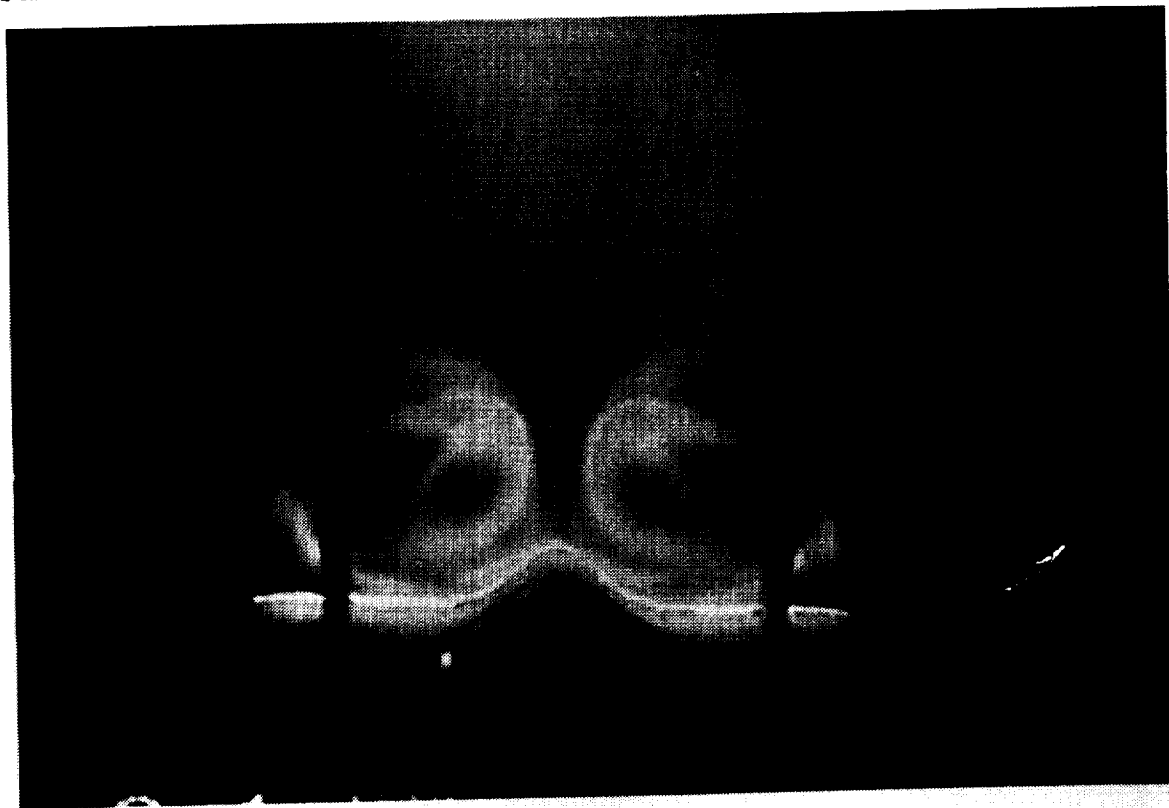
0° LEF
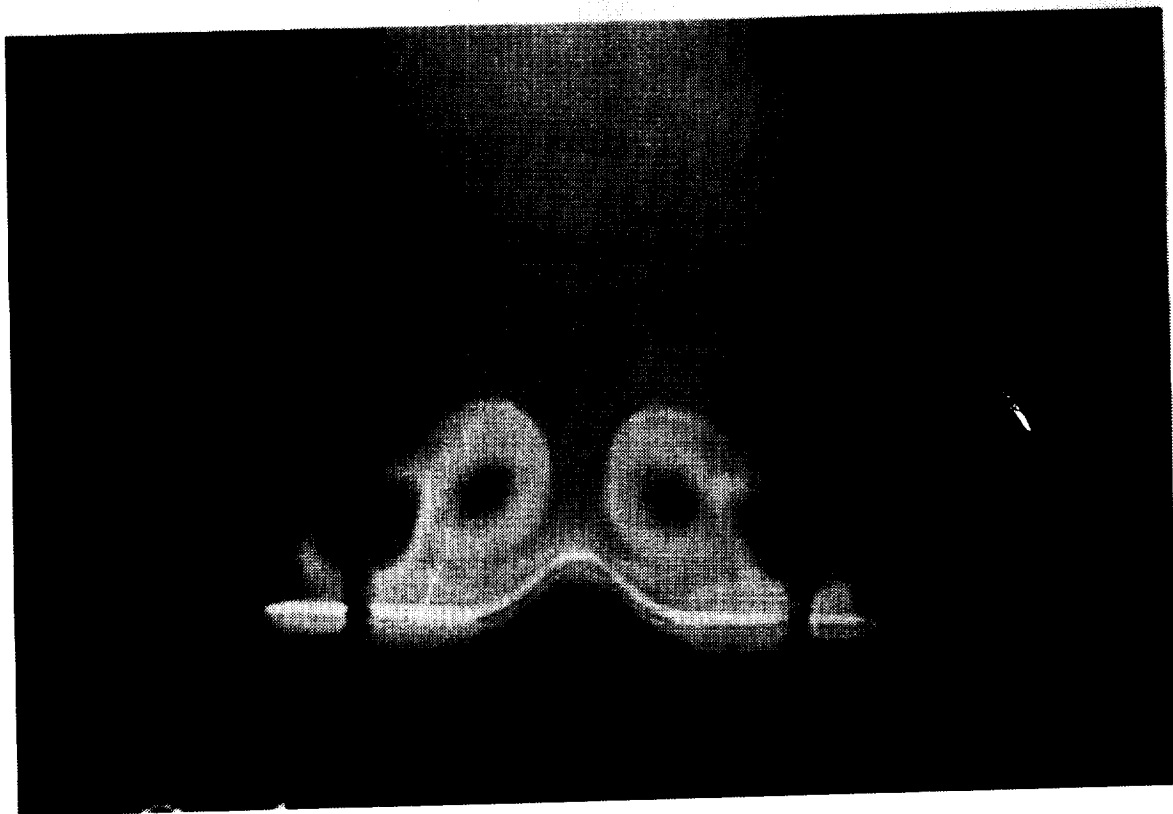
2/3-span
30° LEF

Fig. 10   Vapor screen visualization at $M_\infty = 0.9$; twin-tail configuration; $\alpha = 26°$.

$\beta = 3°$

$\beta = 4.5°$

$\beta = 6°$
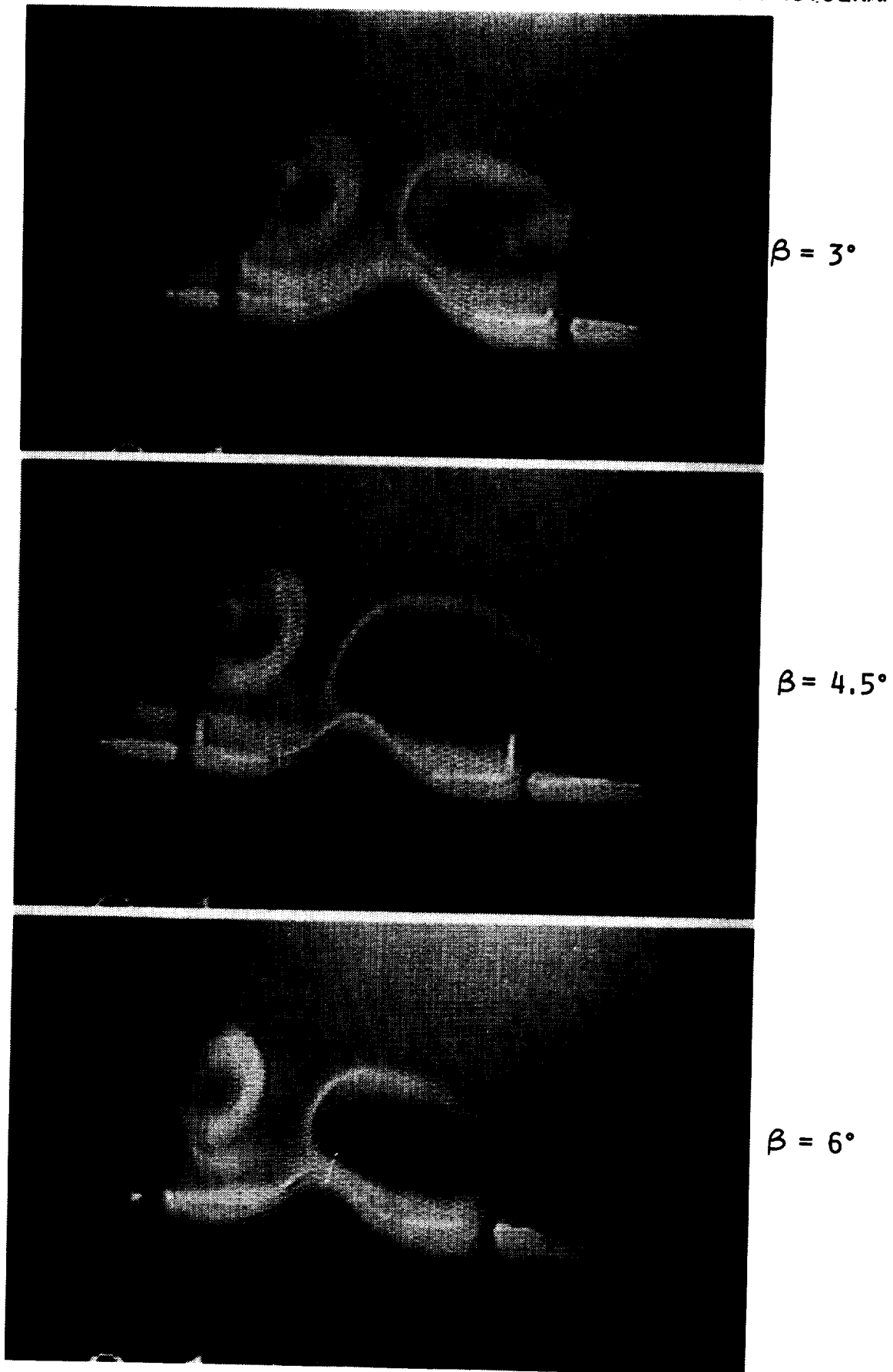
Fig. 11   Vapor screen visualization at $M_\infty = 0.9$; twin-tail configuration in sideslip at $\alpha = 26°$; 0° LEF.

$\beta = 3°$

$\beta = 4.5°$

$\beta = 6°$
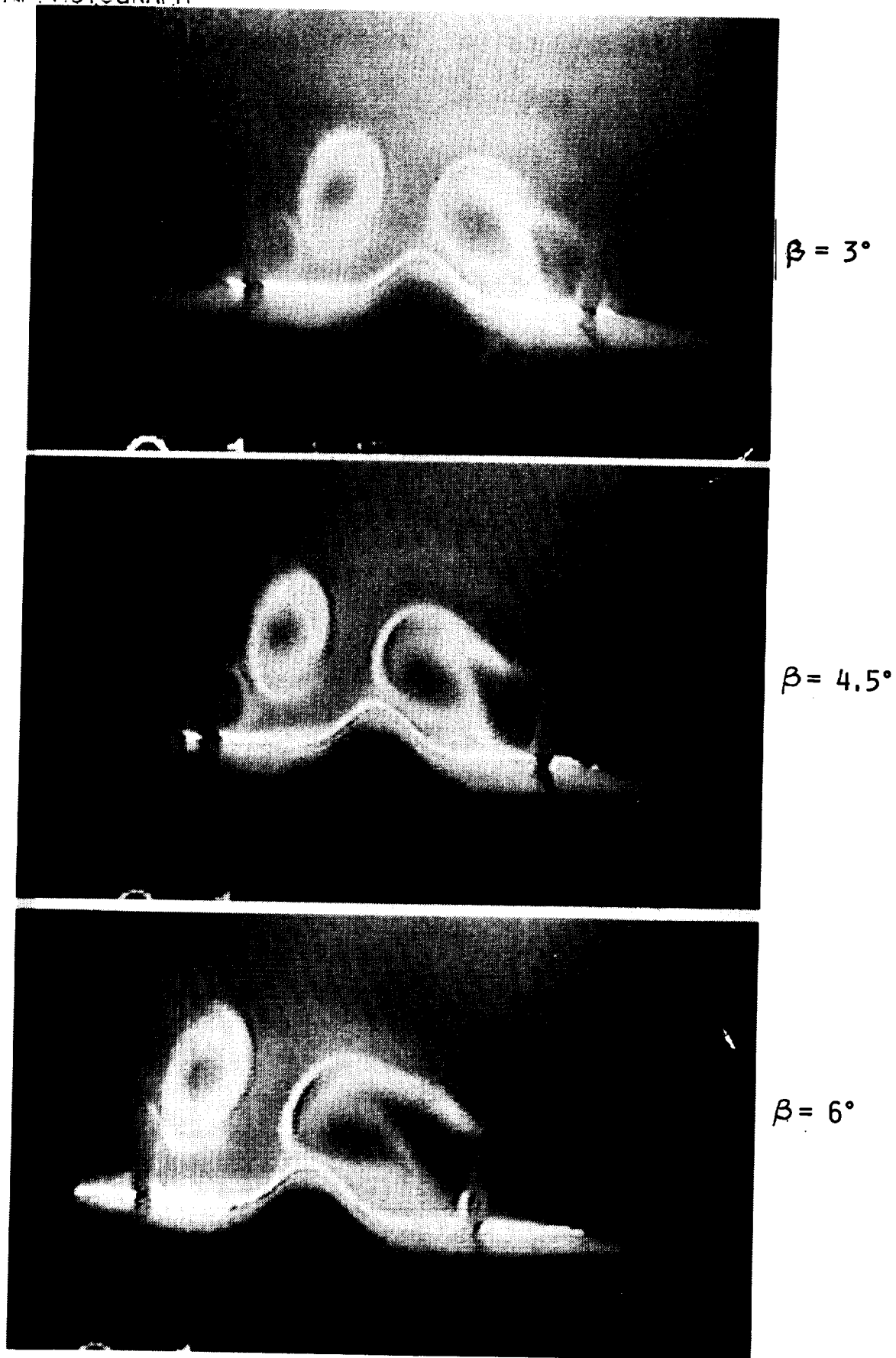
Fig. 12   Vapor screen visualization at M = 0.9; twin-tail configuration in sideslip at $\alpha = 26°$; 2/3-span 30° LEF.

27
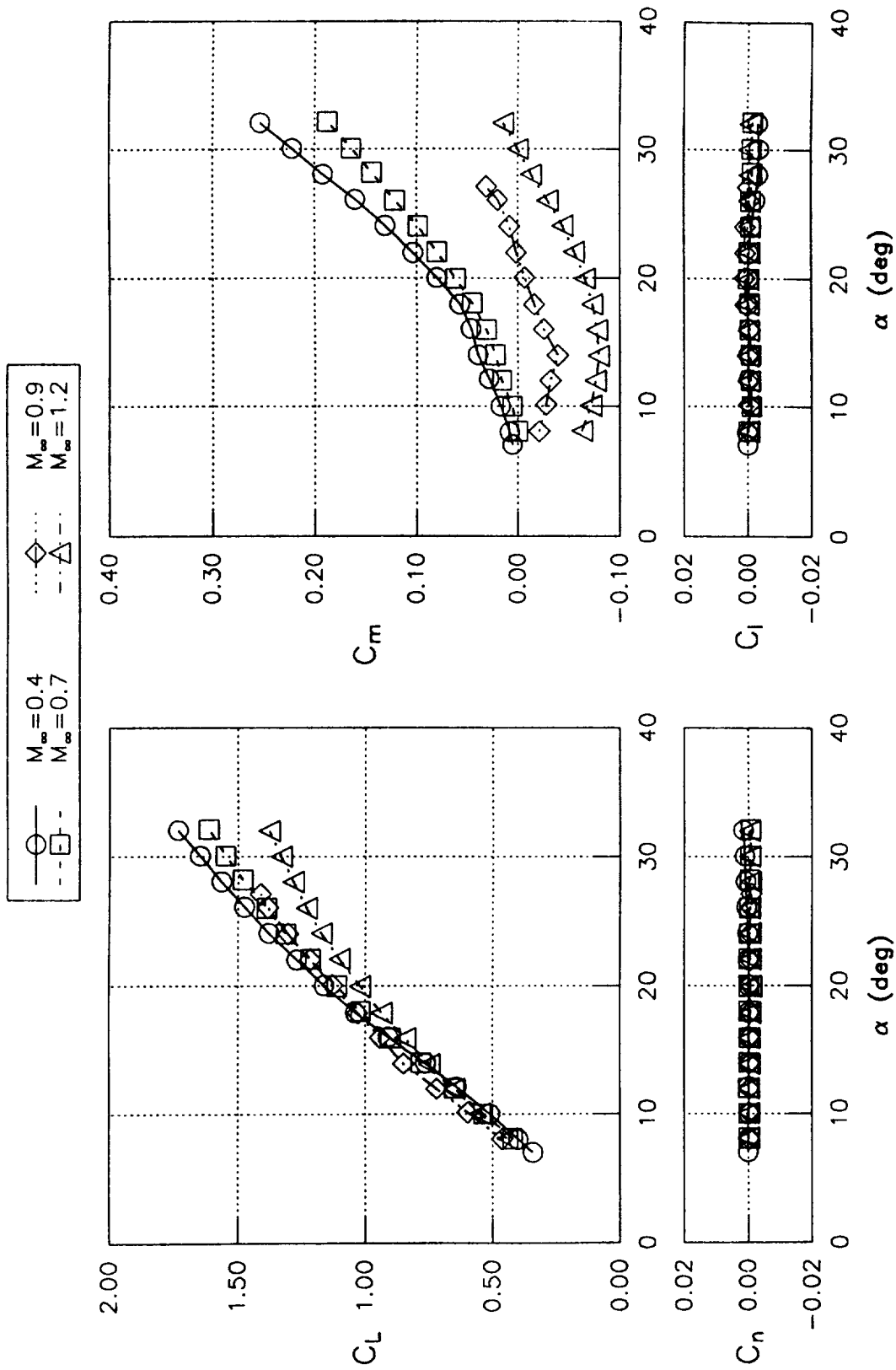
Fig. 13   Lift and moment characteristics of tail-off, 0° LEF configuration at various Mach numbers, β = 0°.

28
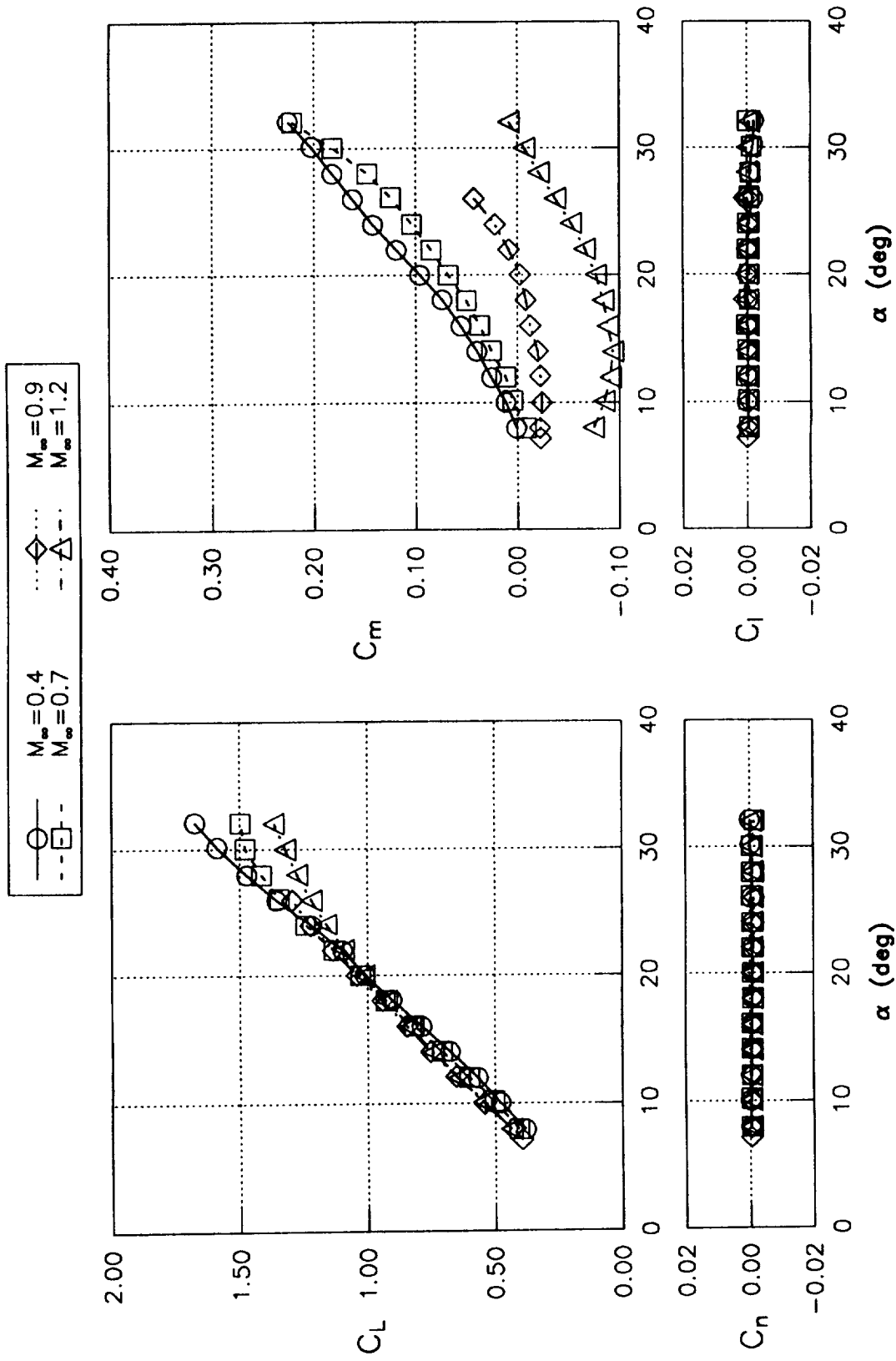
Fig. 14   Lift and moment characteristics of tail-off, 1/3-span 30° LEF configuration at various Mach numbers, ß = 0°.

29
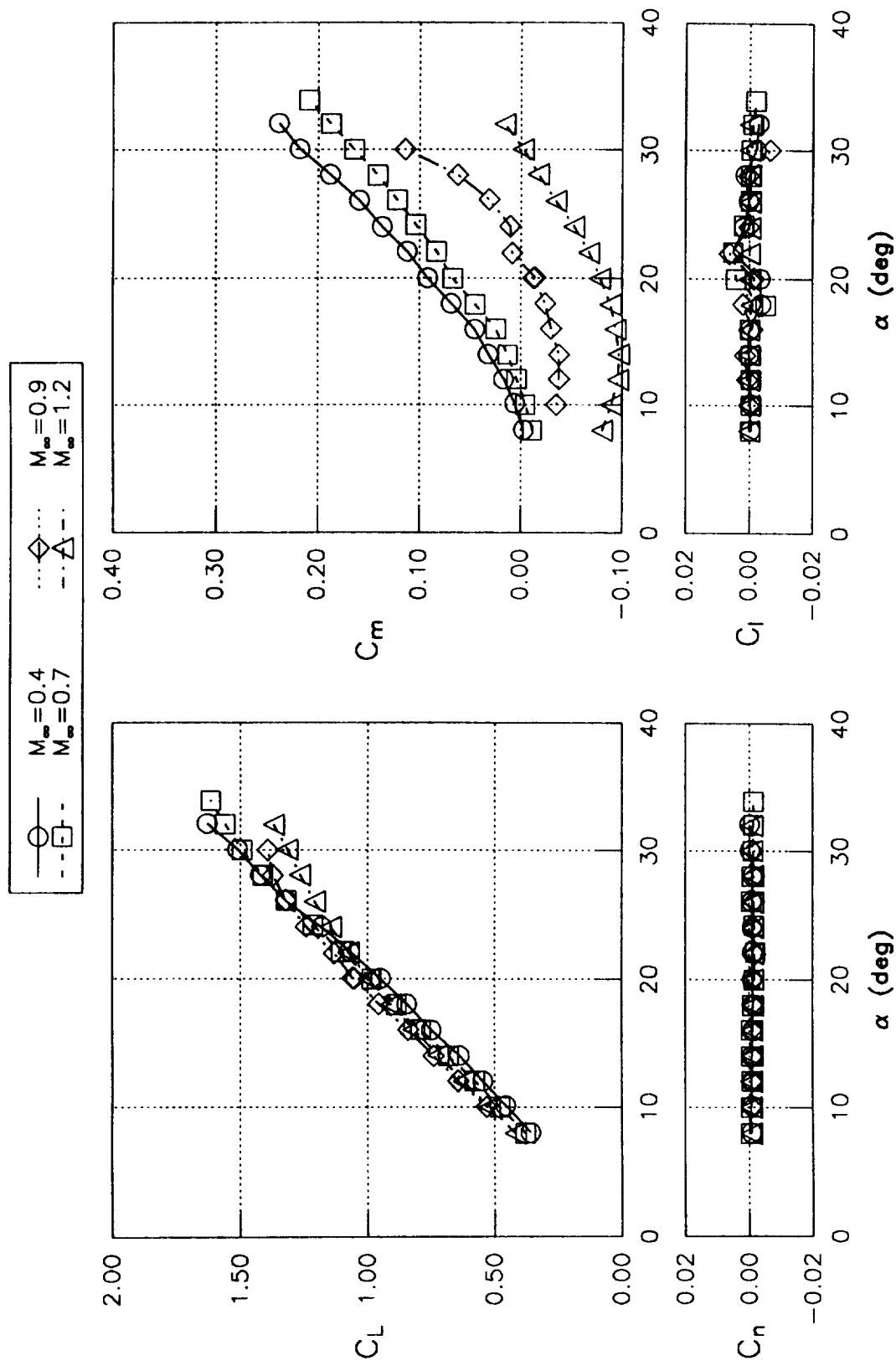
Fig. 15   Lift and moment characteristics of tail-off, 2/3-span 30° LEF configuration at various Mach numbers, ß = 0°.
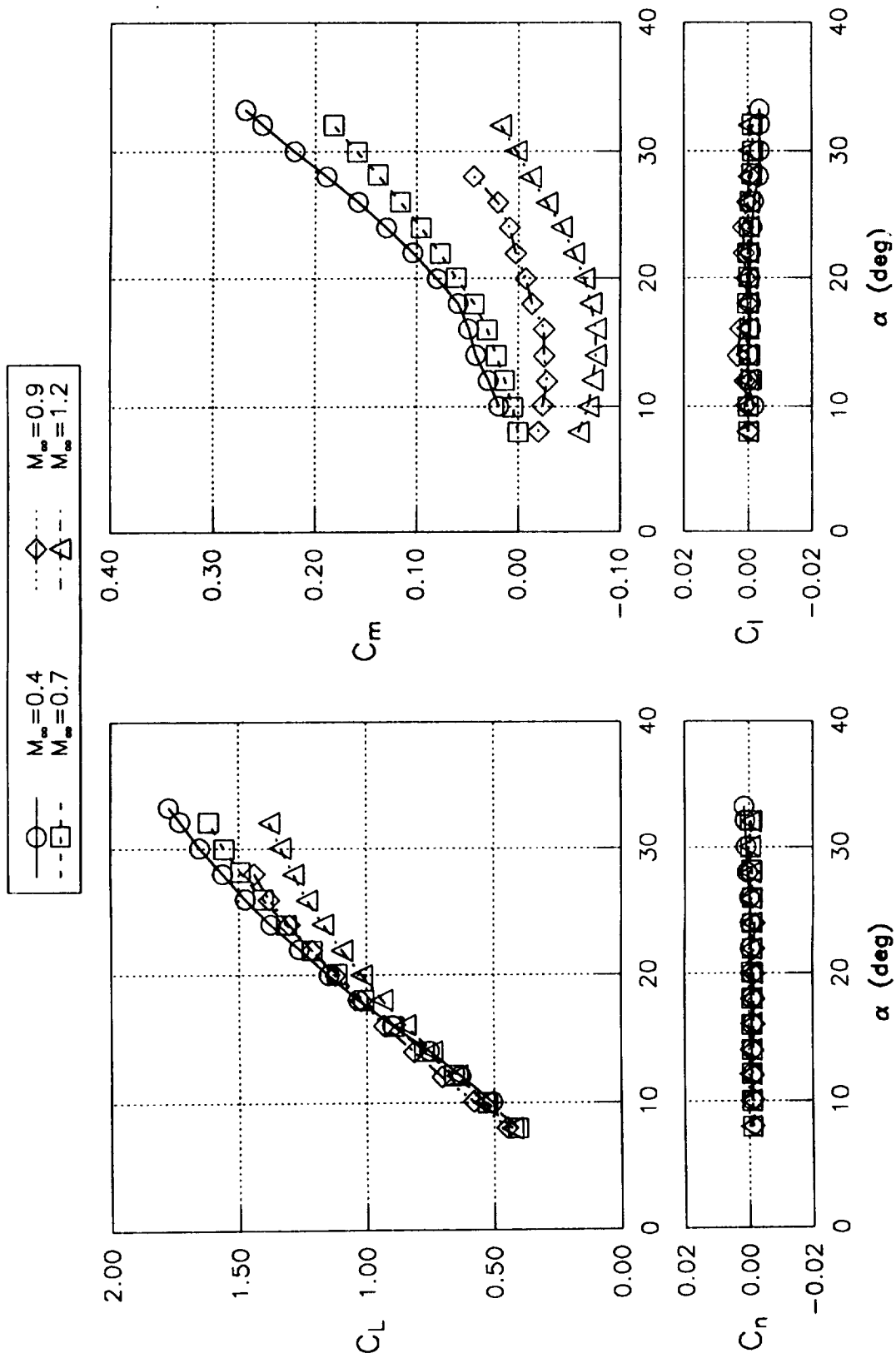
Fig. 16   Lift and moment characteristics of central-tail, 0° LEF
configuration at various Mach numbers, ß = 0°.

31
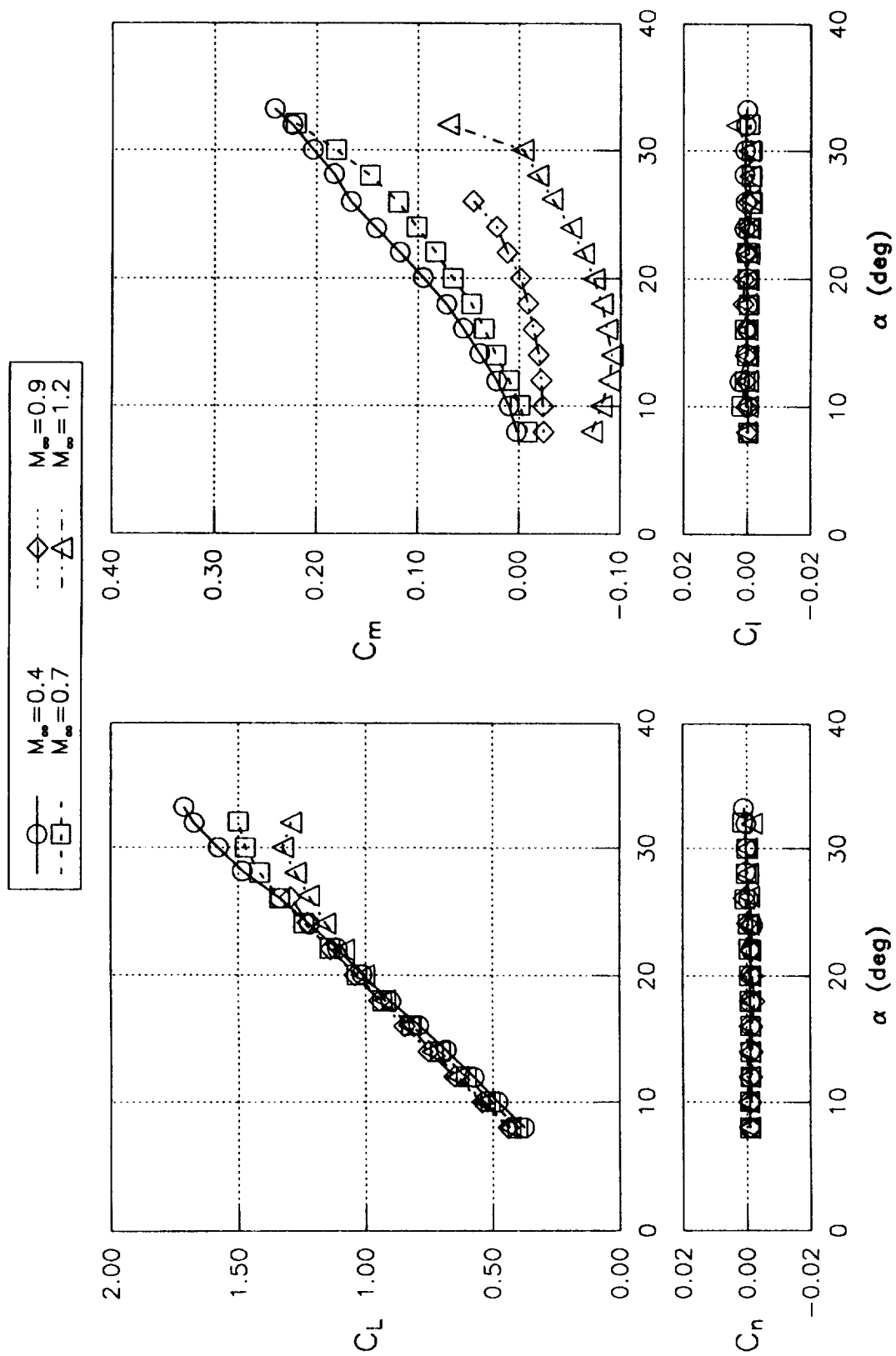
Fig. 17   Lift and moment characteristics of central-tail, 1/3-span 30°
LEF configuration at various Mach numbers, ß = 0°.
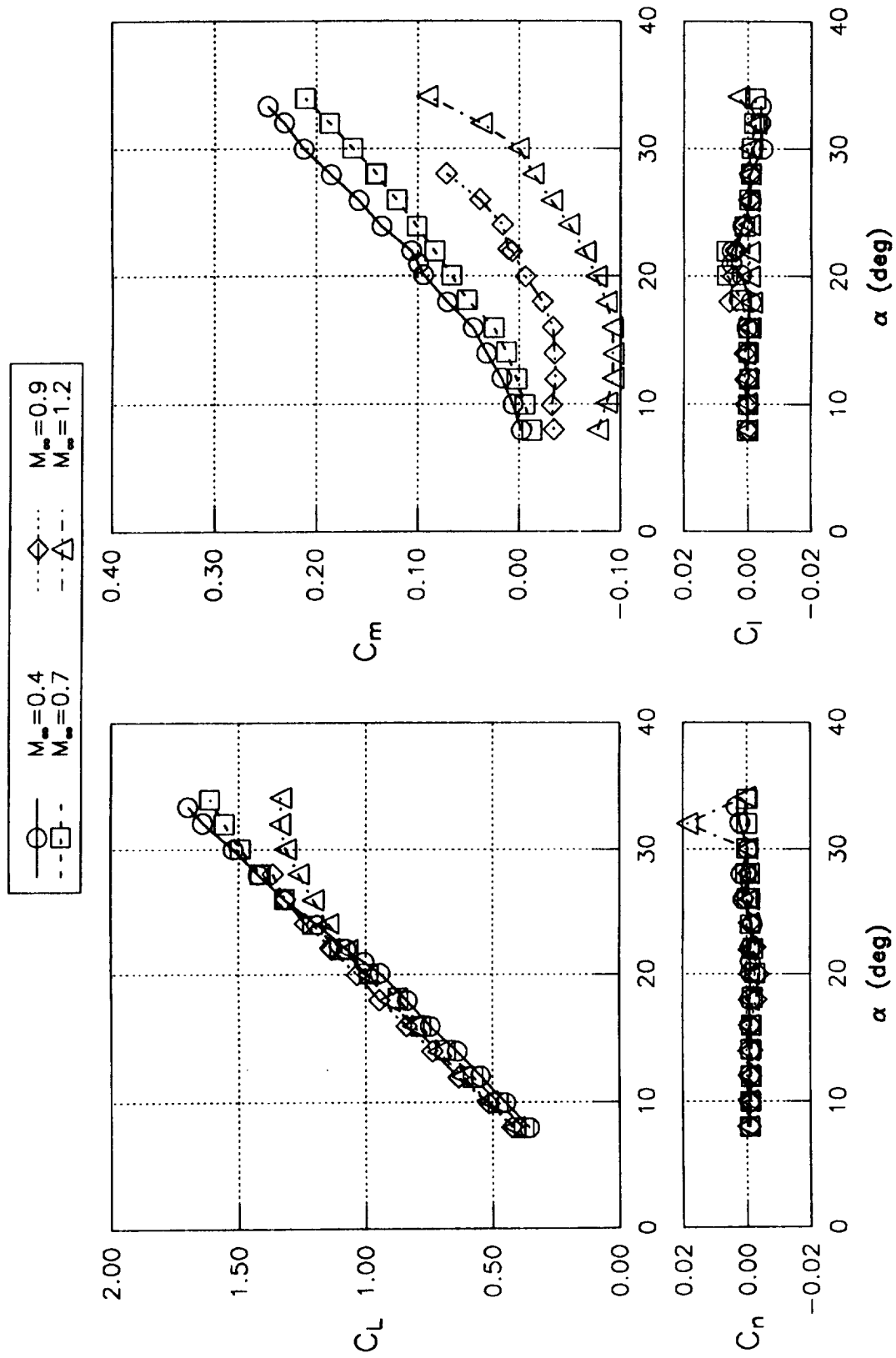
Fig. 18   Lift and moment characteristics of central-tail, 2/3-span 30°
LEF configuration at various Mach numbers, ß = 0°.

33
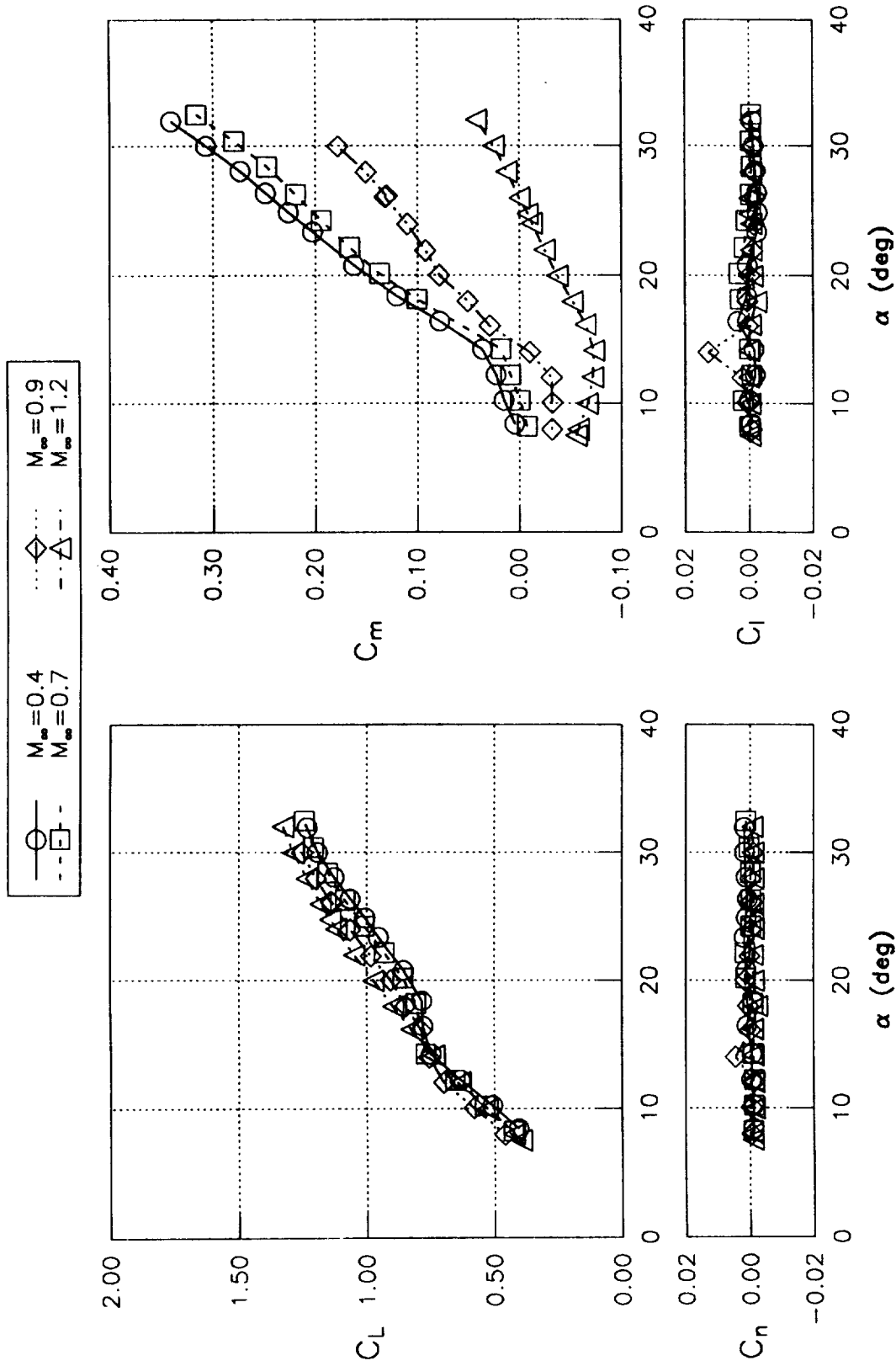
Fig. 19   Lift and moment characteristics of twin-tail, 0° LEF configuration at various Mach numbers, ß = 0°.
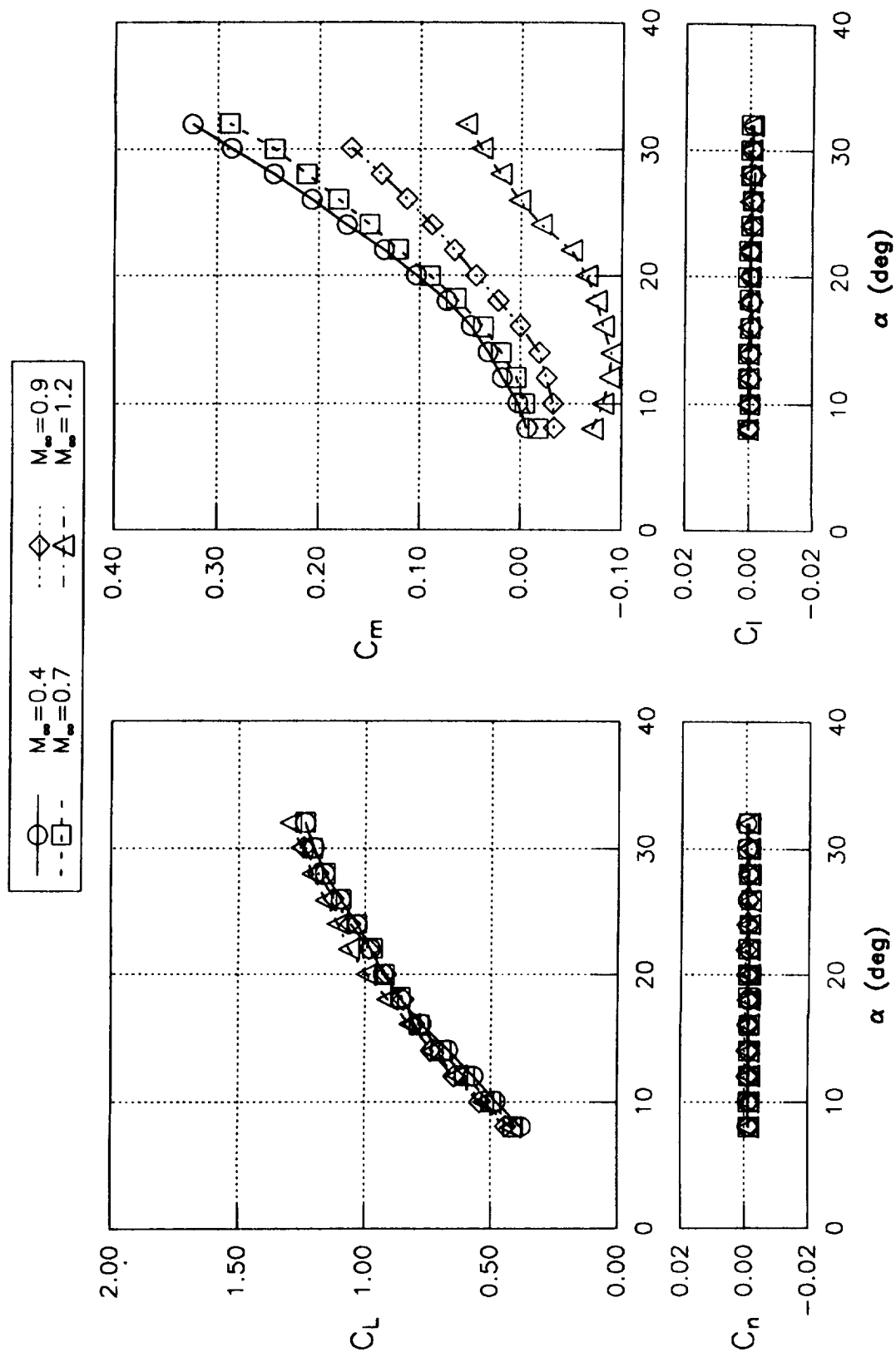
Fig. 20   Lift and moment characteristics of twin-tail, 1/3-span 30° LEF
configuration at various Mach numbers, ß = 0°.

35
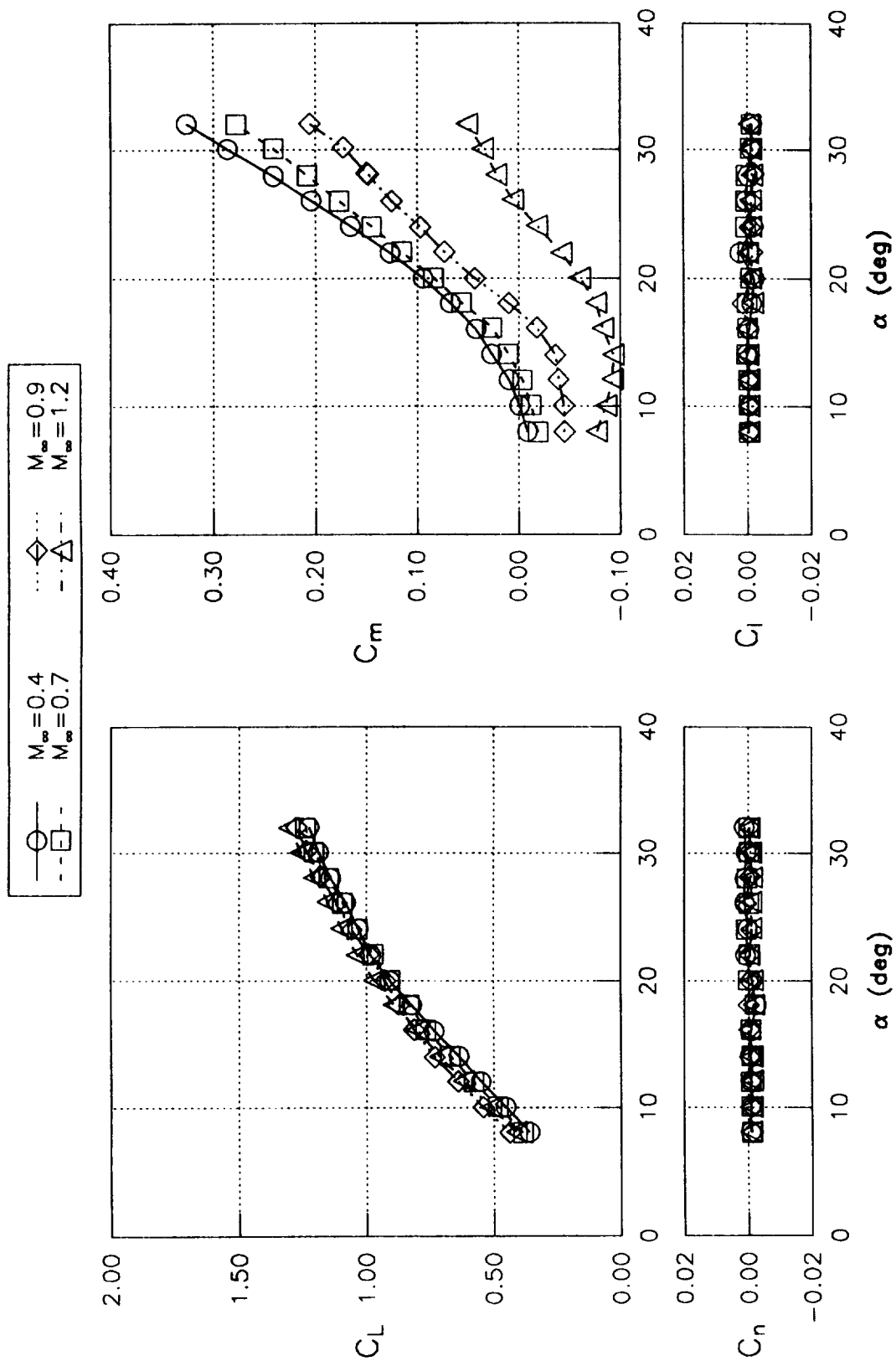
Fig. 21   Lift and moment characteristics of twin-tail, 2/3-span 30° LEF configuration at various Mach numbers, ß = 0°.
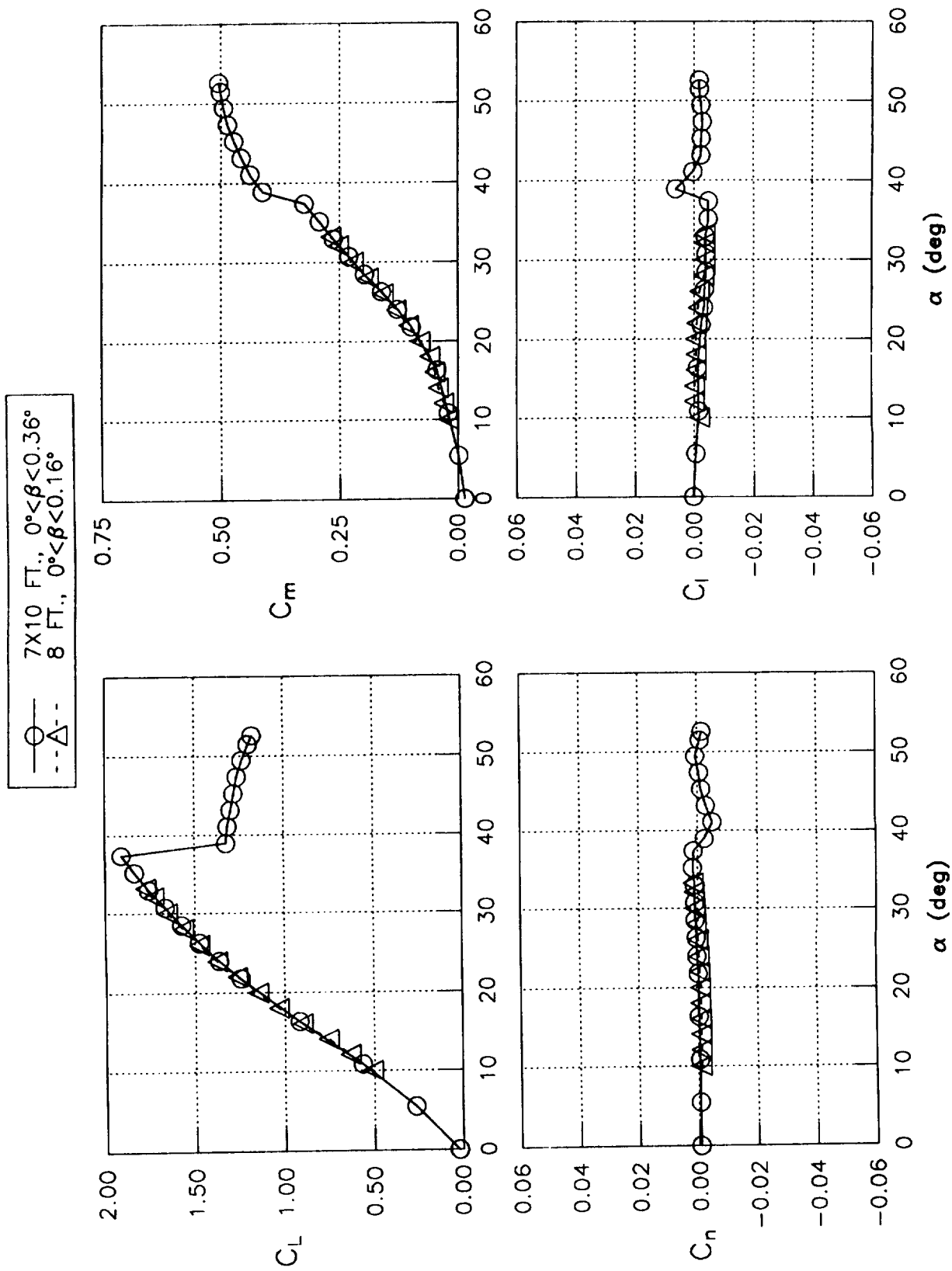
Fig. 22   7- by 10-Foot HST and 8-Foot TPT data comparisons of lift and moment characteristics; central-tail, 0° LEF configuration, $M_\infty = 0.4$.
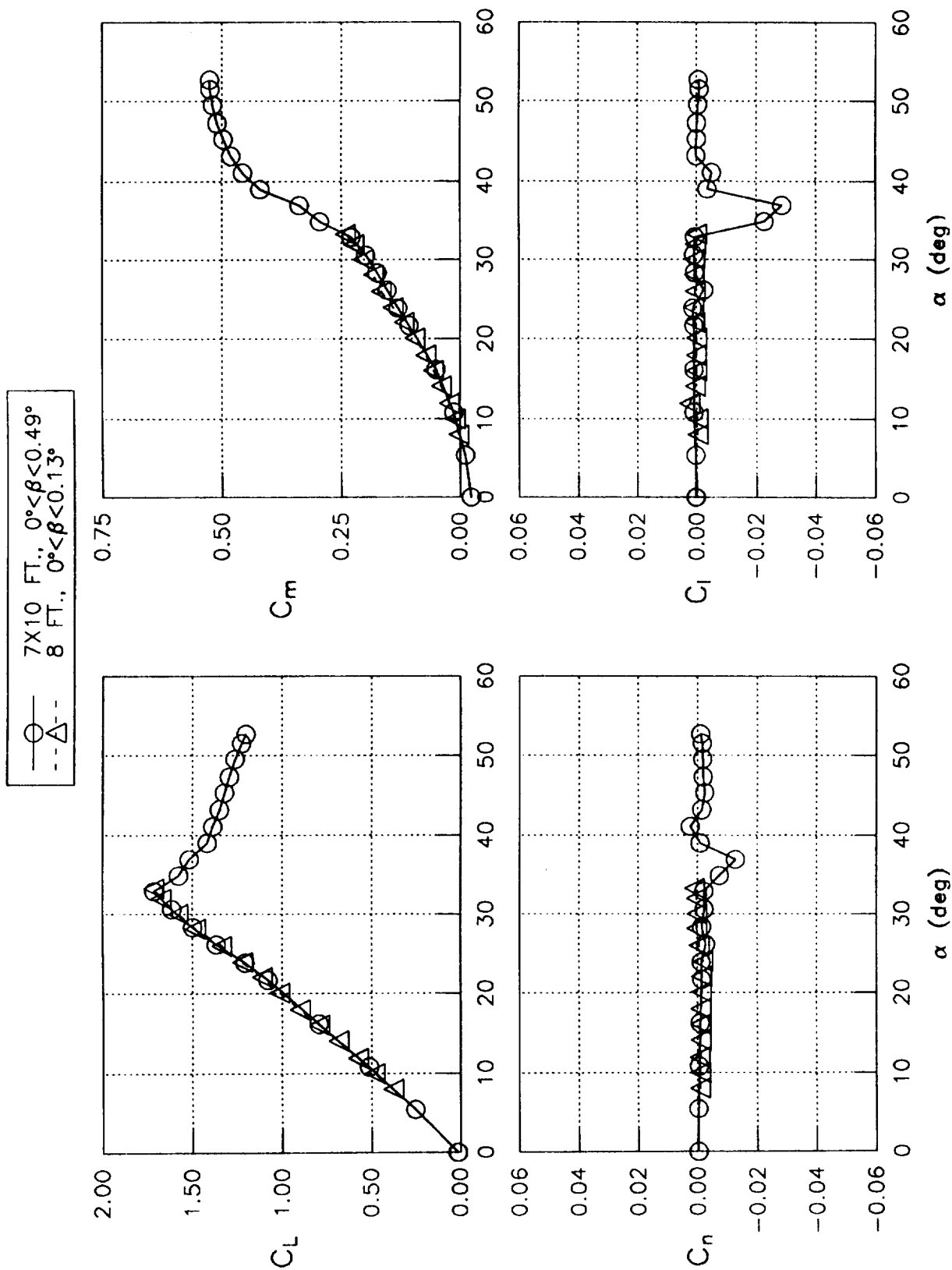
Fig. 23 7- by 10-Foot HST and 8-Foot TPT data comparisons of lift and moment characteristics; central-tail, 1/3-span 30° LEF configuration, M_∞ = 0.4.
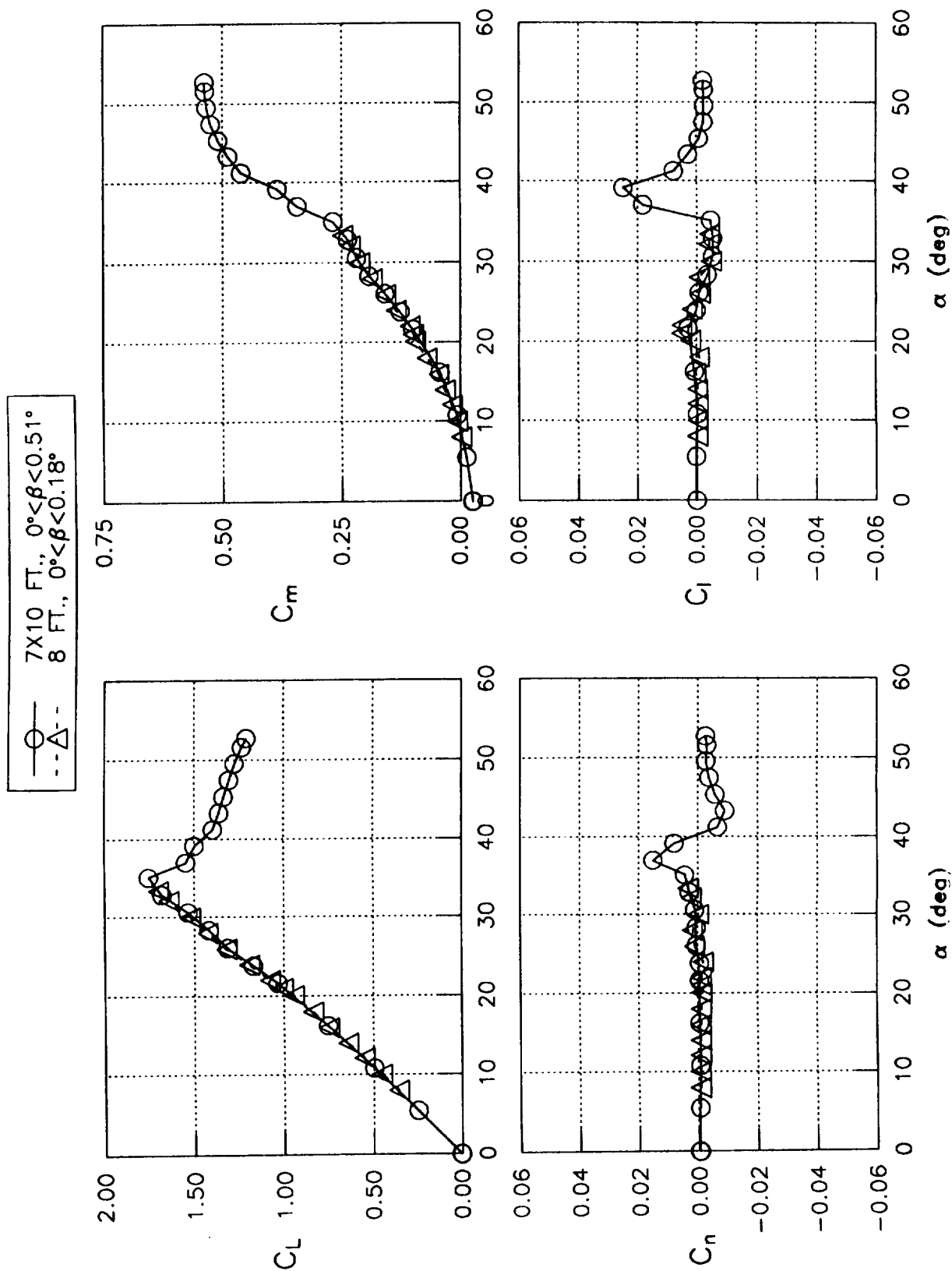
Fig. 24 7- by 10-Foot HST and 8-Foot TPT data comparisons of lift and moment characteristics; central-tail, 2/3-span 30° LEF configuration, $M_\infty = 0.4$.
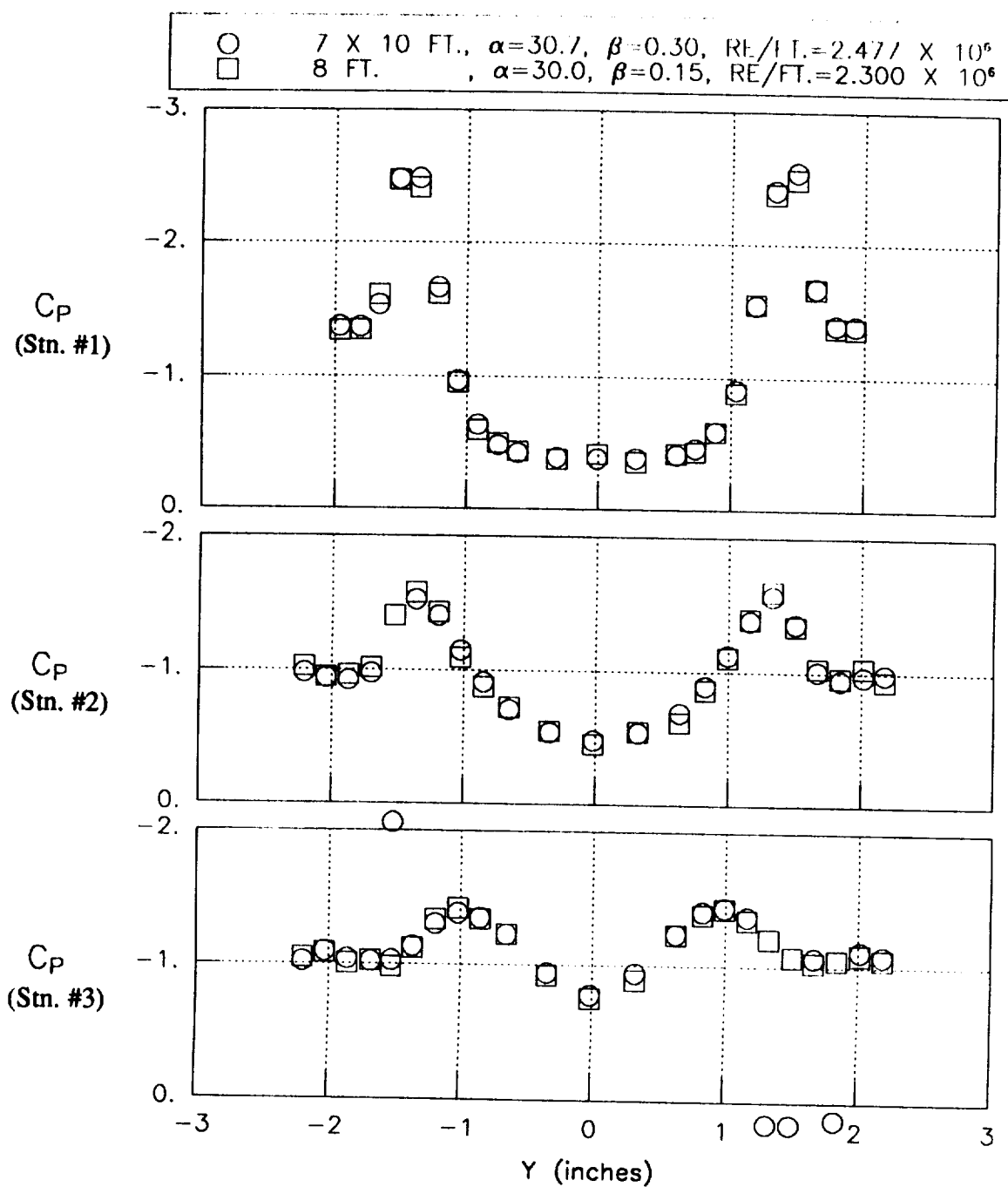
Fig. 25   Comparison of 7- by 10-Foot HST and 8-Foot TPT M_∞ = 0.4 test
data. Forebody pressure distributions at α = 30°, C.V.T.; 0° LEF.

40
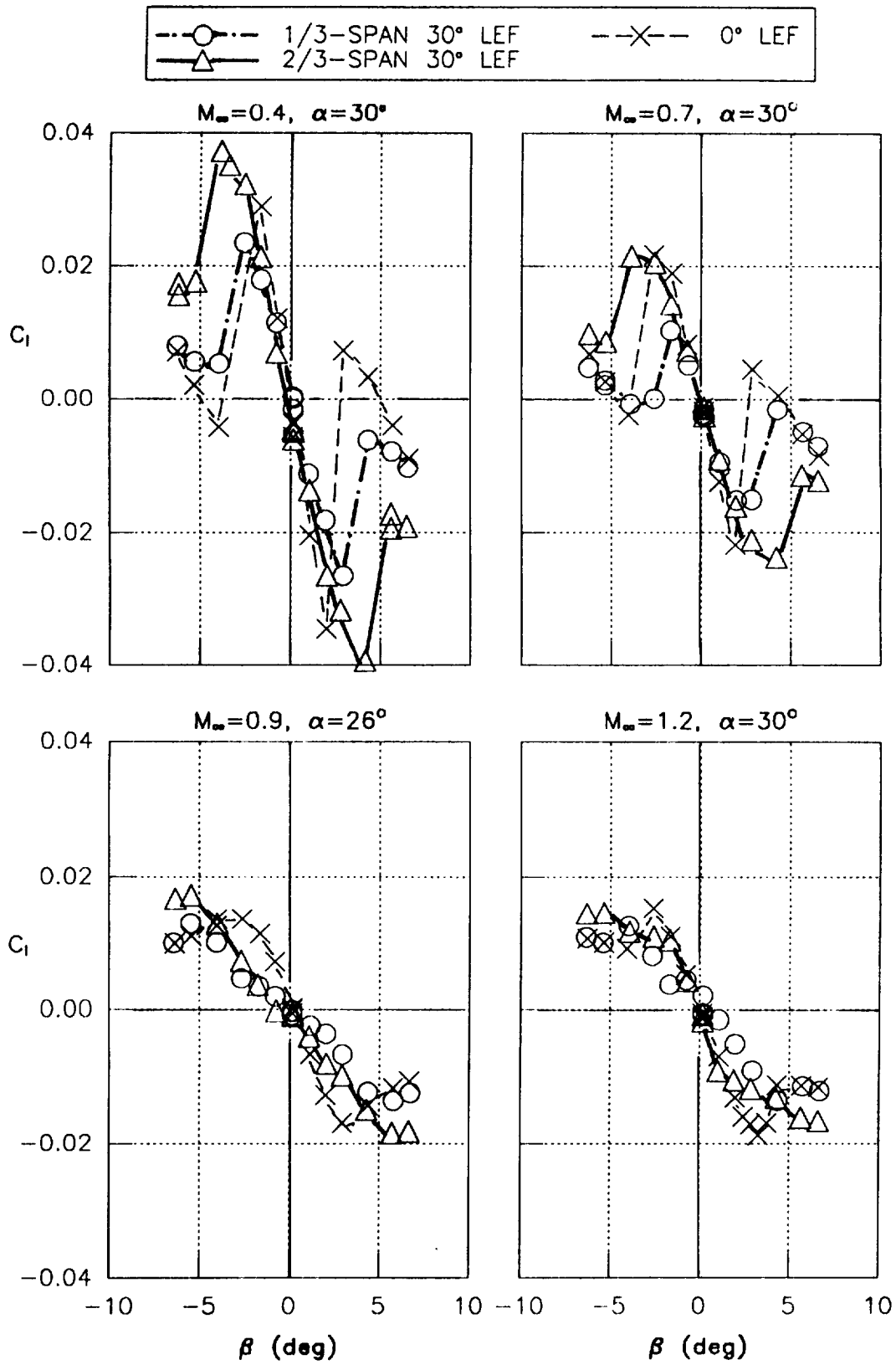
Fig. 26   Lateral characteristics versus sideslip angle at α = 30°, showing flap effect at various Mach numbers, C.V.T.

Fig. 27   Directional characteristics versus sideslip angle at $\alpha = 30°$, showing flap effect
at various Mach numbers, C.V.T.
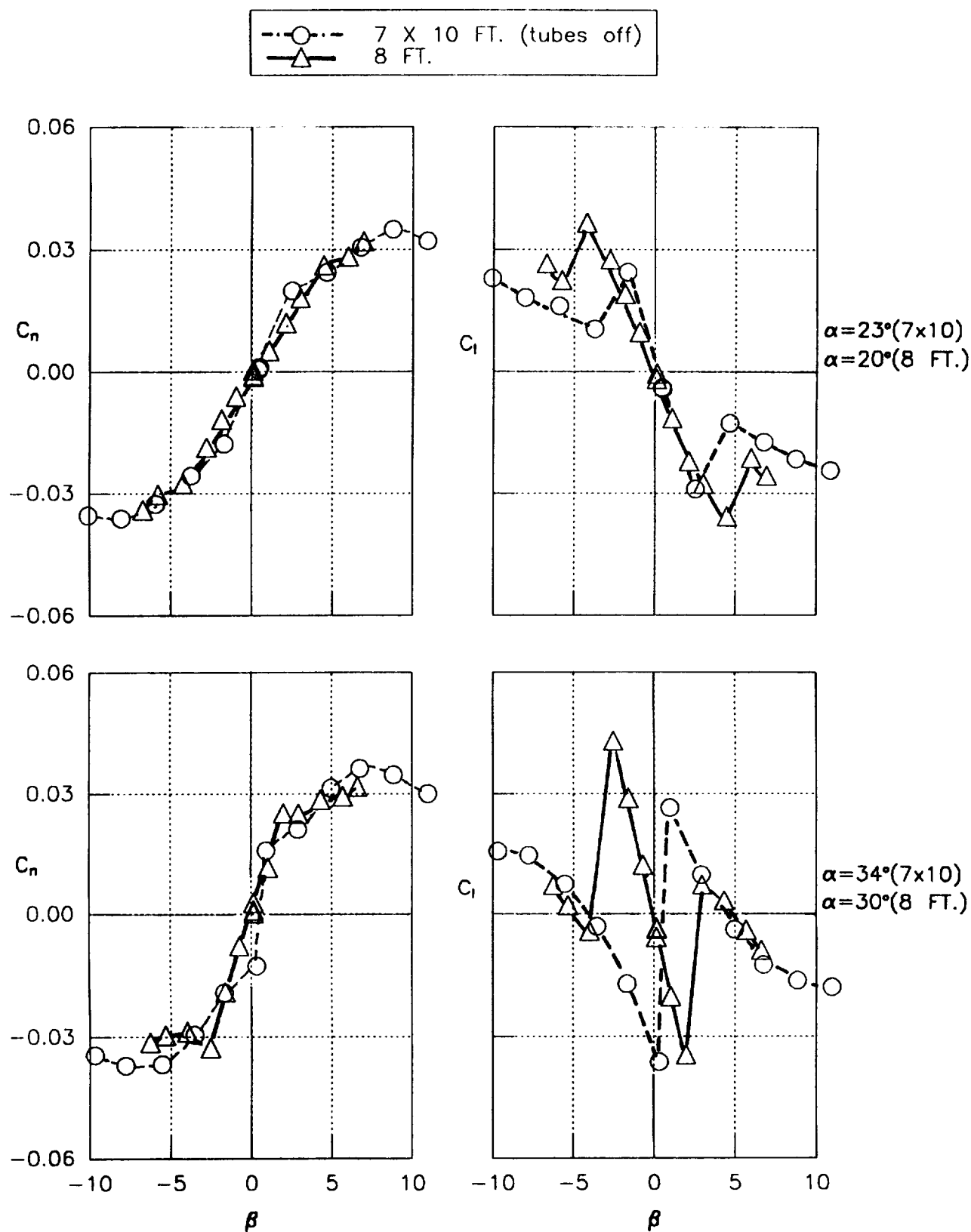
Fig. 28   Comparison of 7- by 10-Foot HST and 8-Foot TPT M_∞ = 0.4 test
data - lateral/directional characteristics at nominal α = 20° and 30°, 0° LEF,
C.V.T.
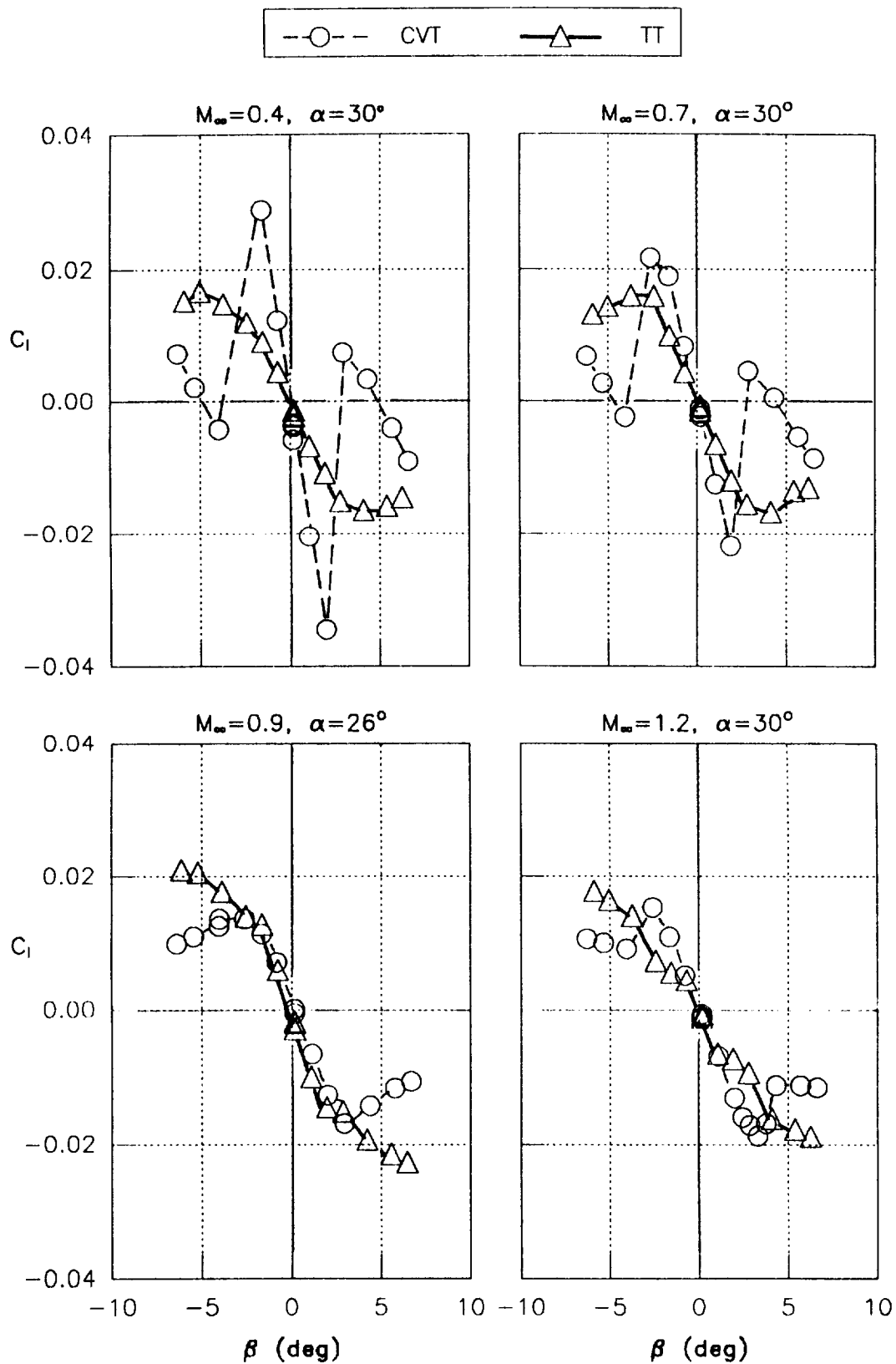
Fig. 29   Comparison of central tail and twin tails lateral characteristics
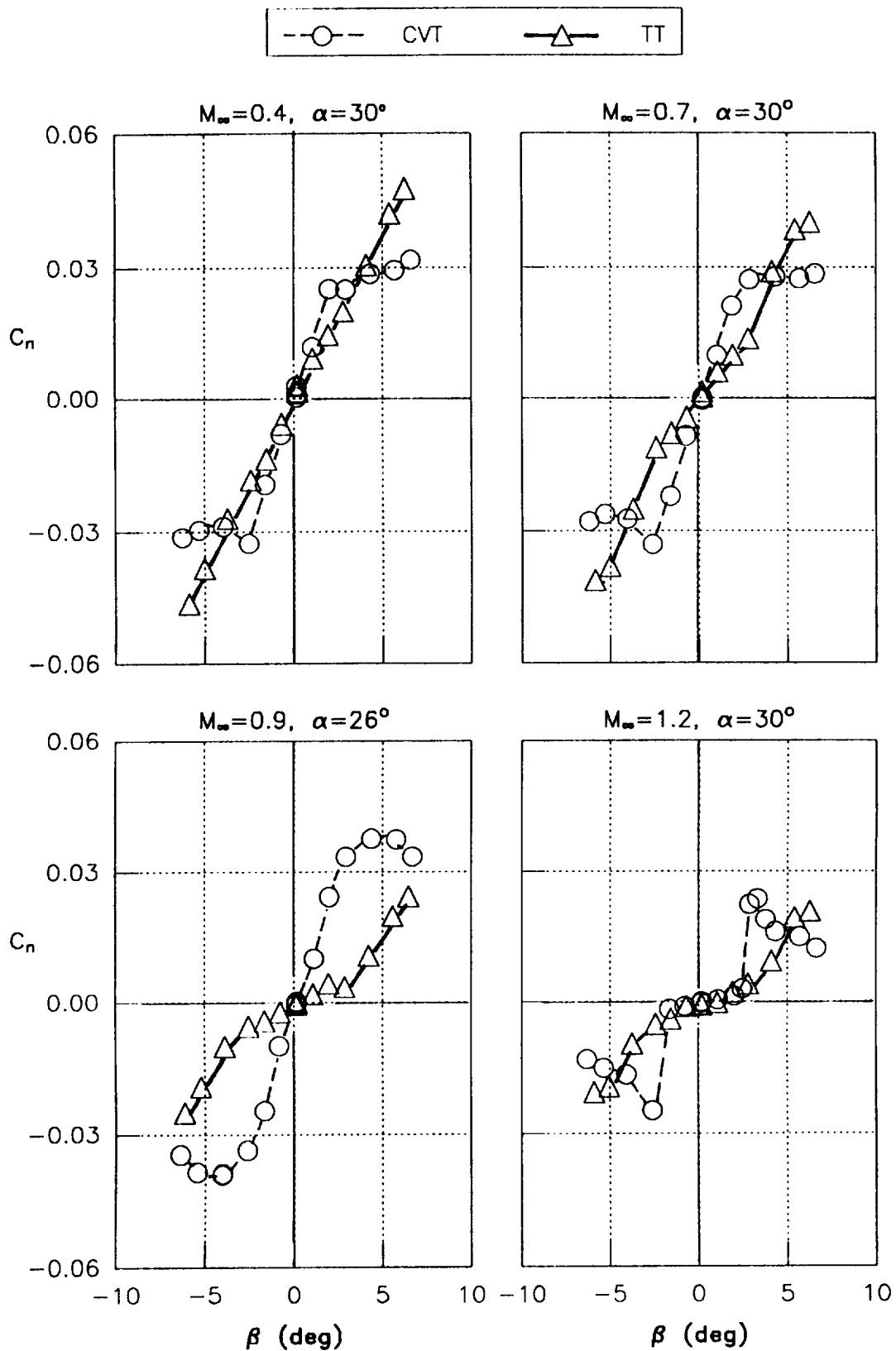   at α = 30° and various Mach numbers, 0° LEF.

Fig. 30   Comparison of central tail and twin tail directional characteristics
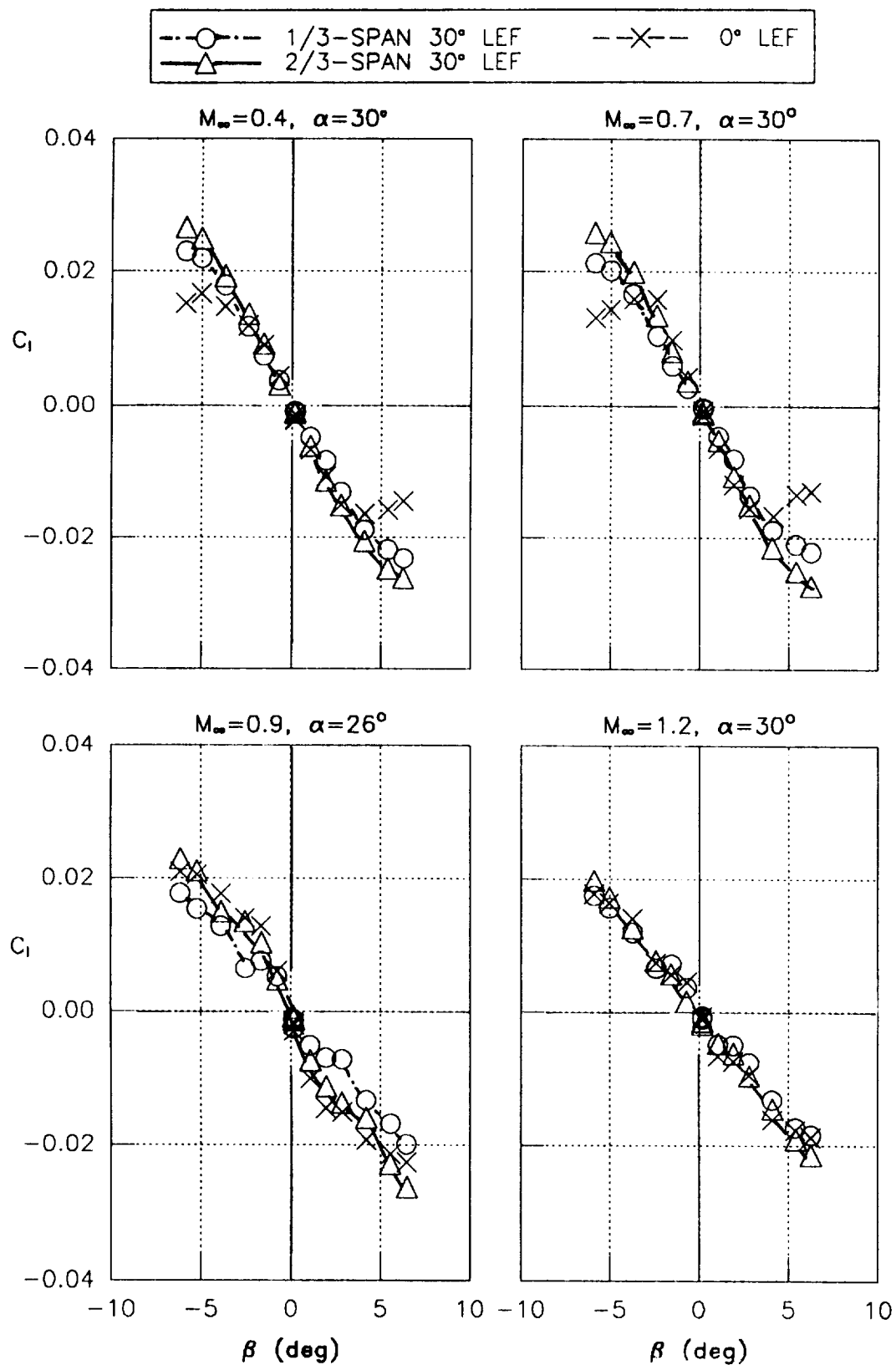at $\alpha = 30°$ and various Mach numbers, $0°$ LEF.

Fig. 31   Lateral characteristics versus sideslip angle with twin tail at α = 30°, showing flap effect at various Mach numbers.
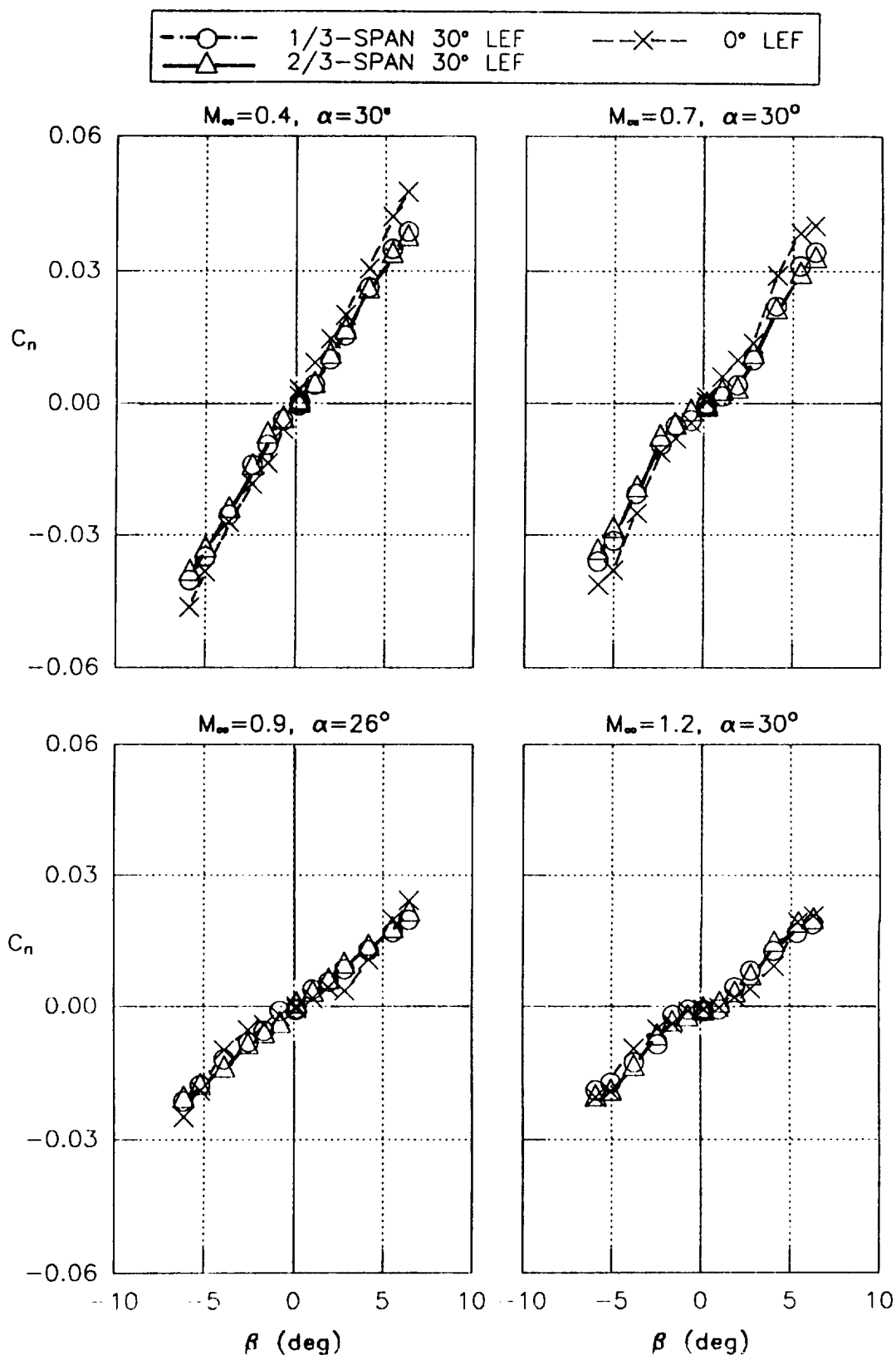
Fig. 32   Directional characteristics versus sideslip angle with twin tail at α = 30°, showing flap effects at various Mach numbers.
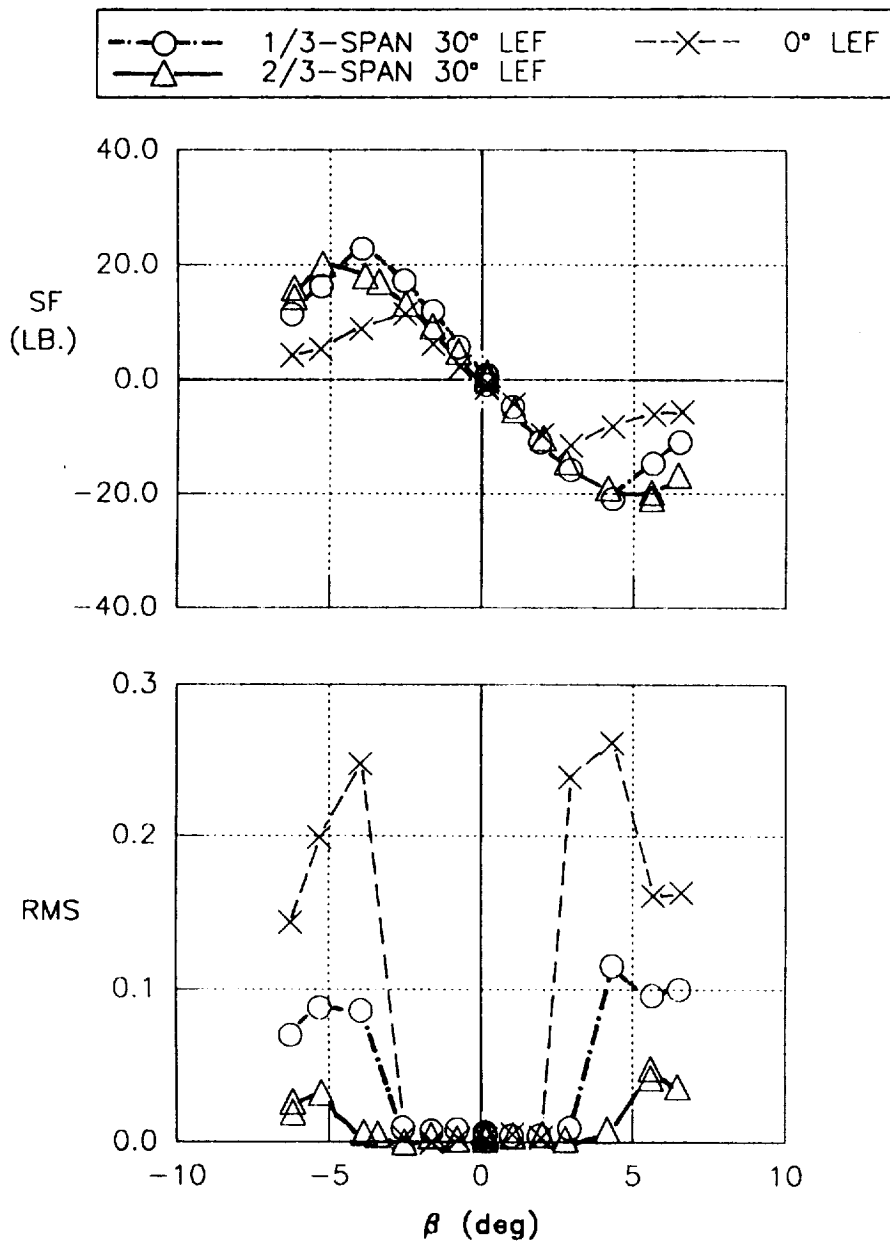
47

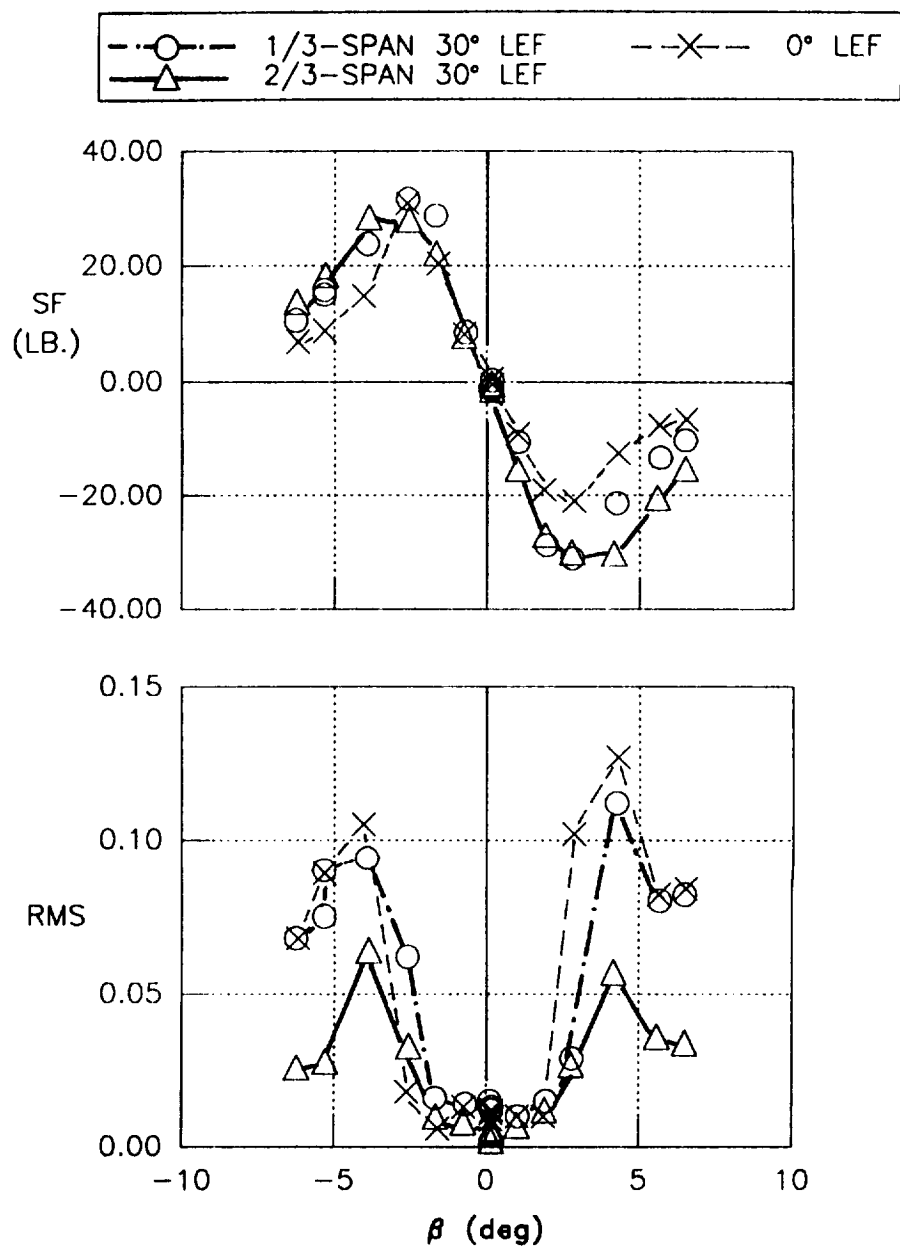Fig. 33   Central tail static and dynamic load characteristics at $\alpha = 30°$, $M_\infty = 0.4$.

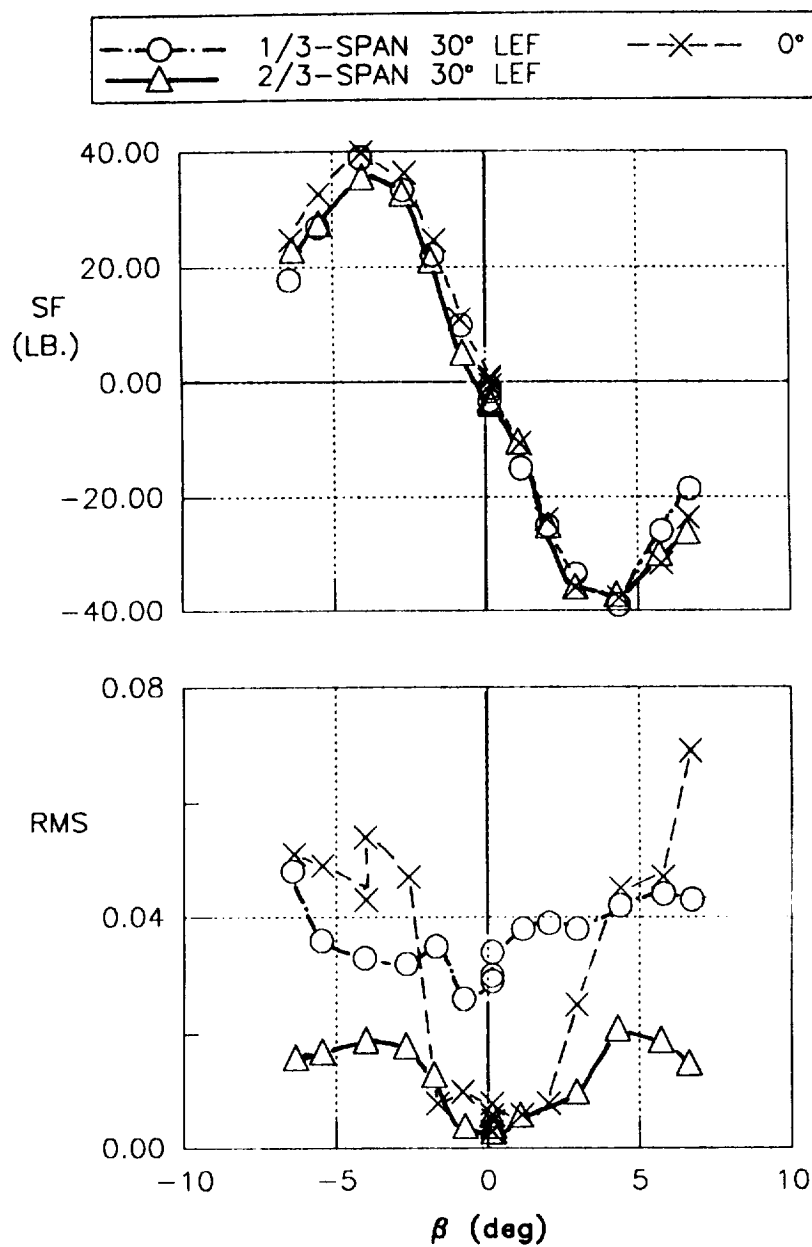Fig. 34   Central tail static and dynamic load characteristics at α = 30°, M_∞ = 0.7.

Fig. 35   Central tail static and dynamic load characteristics at $\alpha = 26°$, $M_\infty = 0.9$.

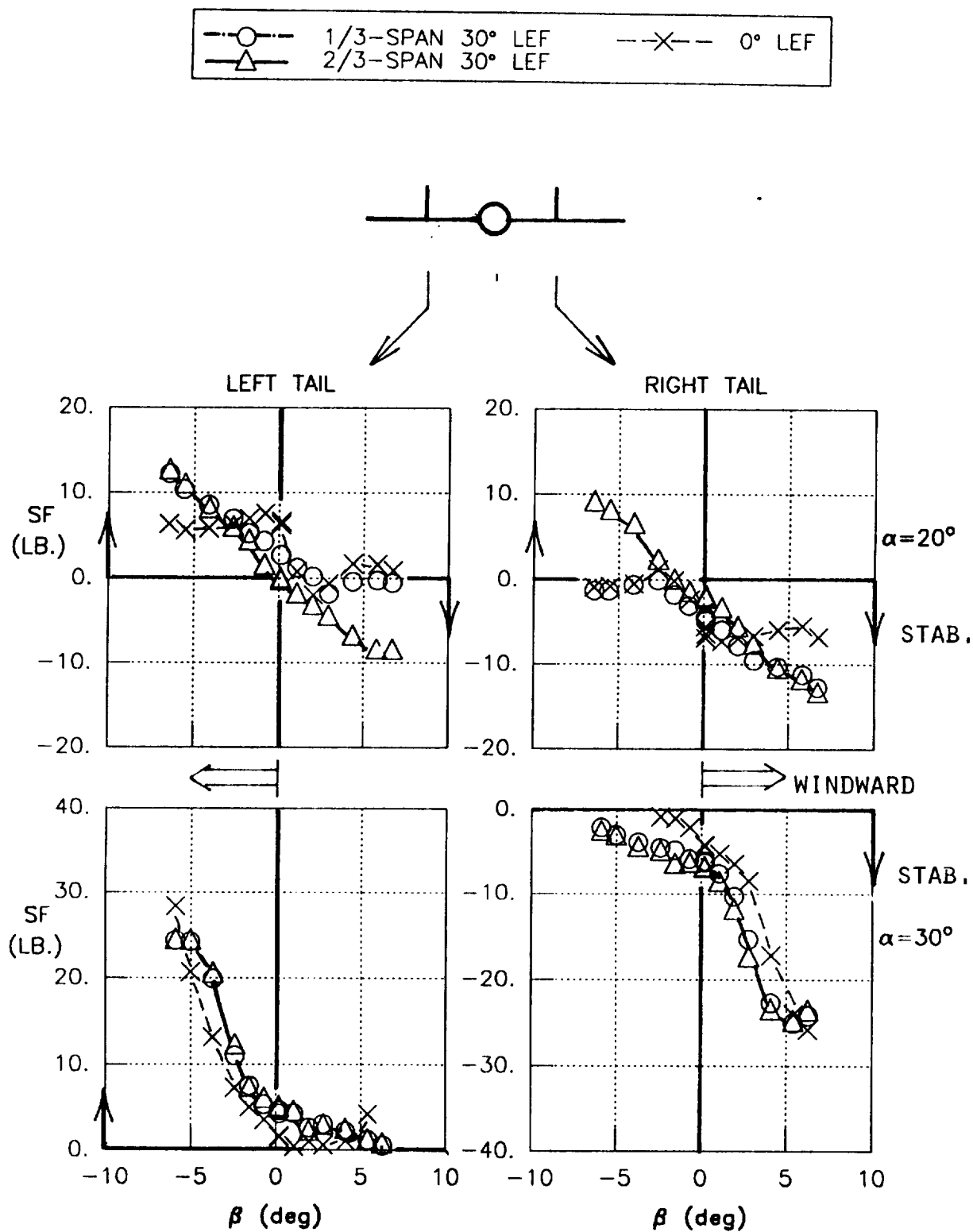Fig. 36   Twin tail static load characteristics at $\alpha = 20°$ and $30°$, $M_\infty = 0.4$.

51

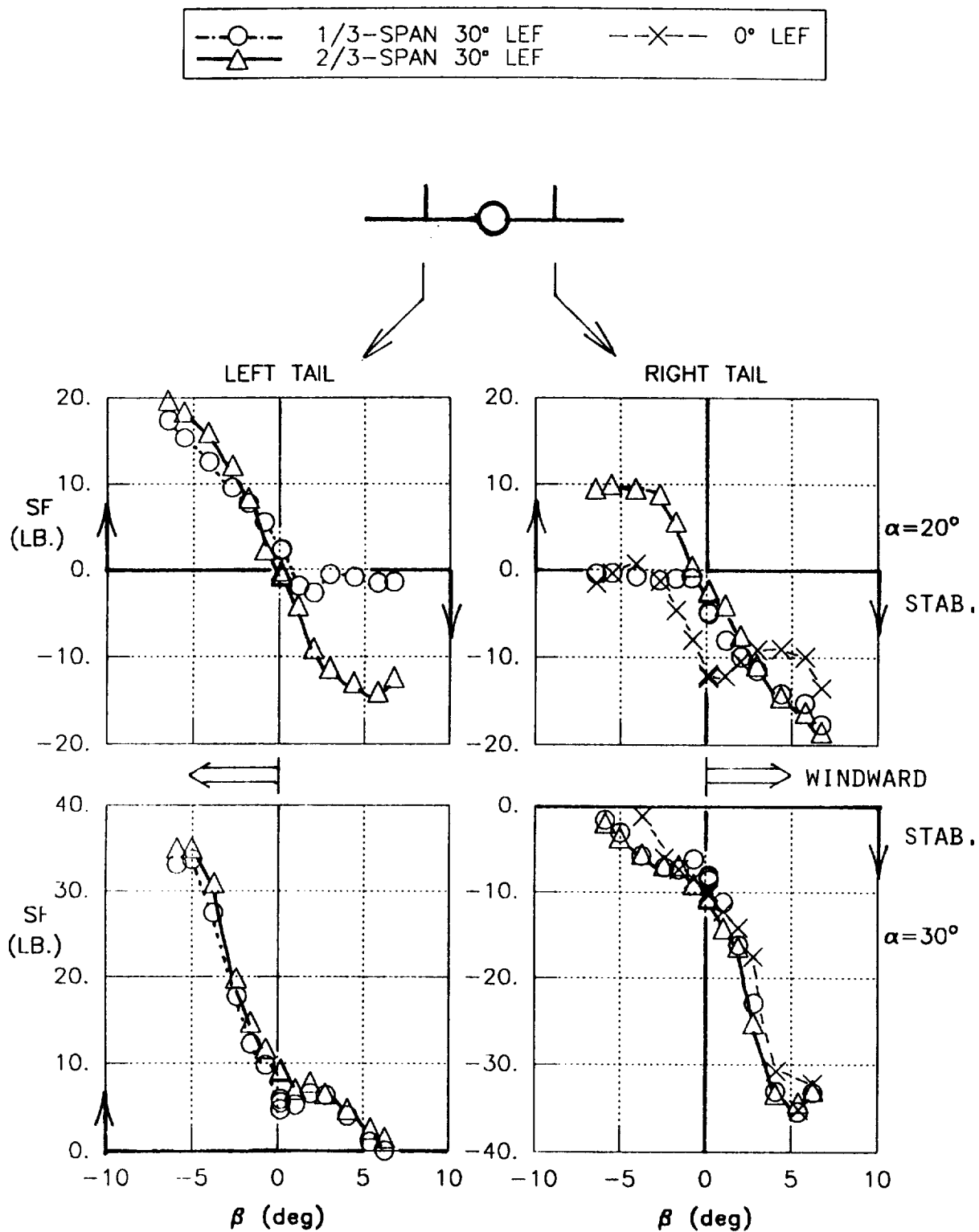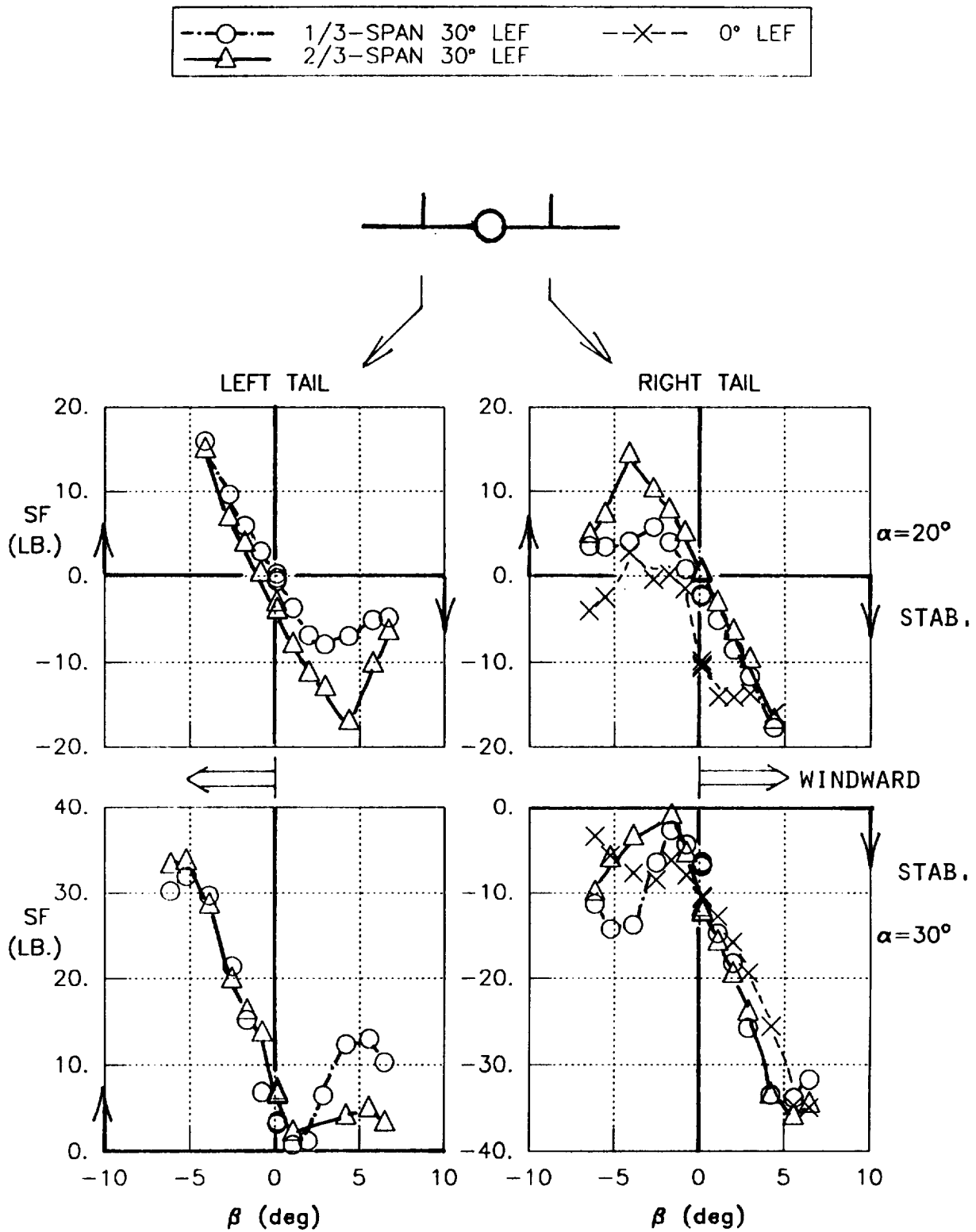**Fig 37** Twin tail static load characteristics at α = 20° and 30°, M_∞ = 0.7.

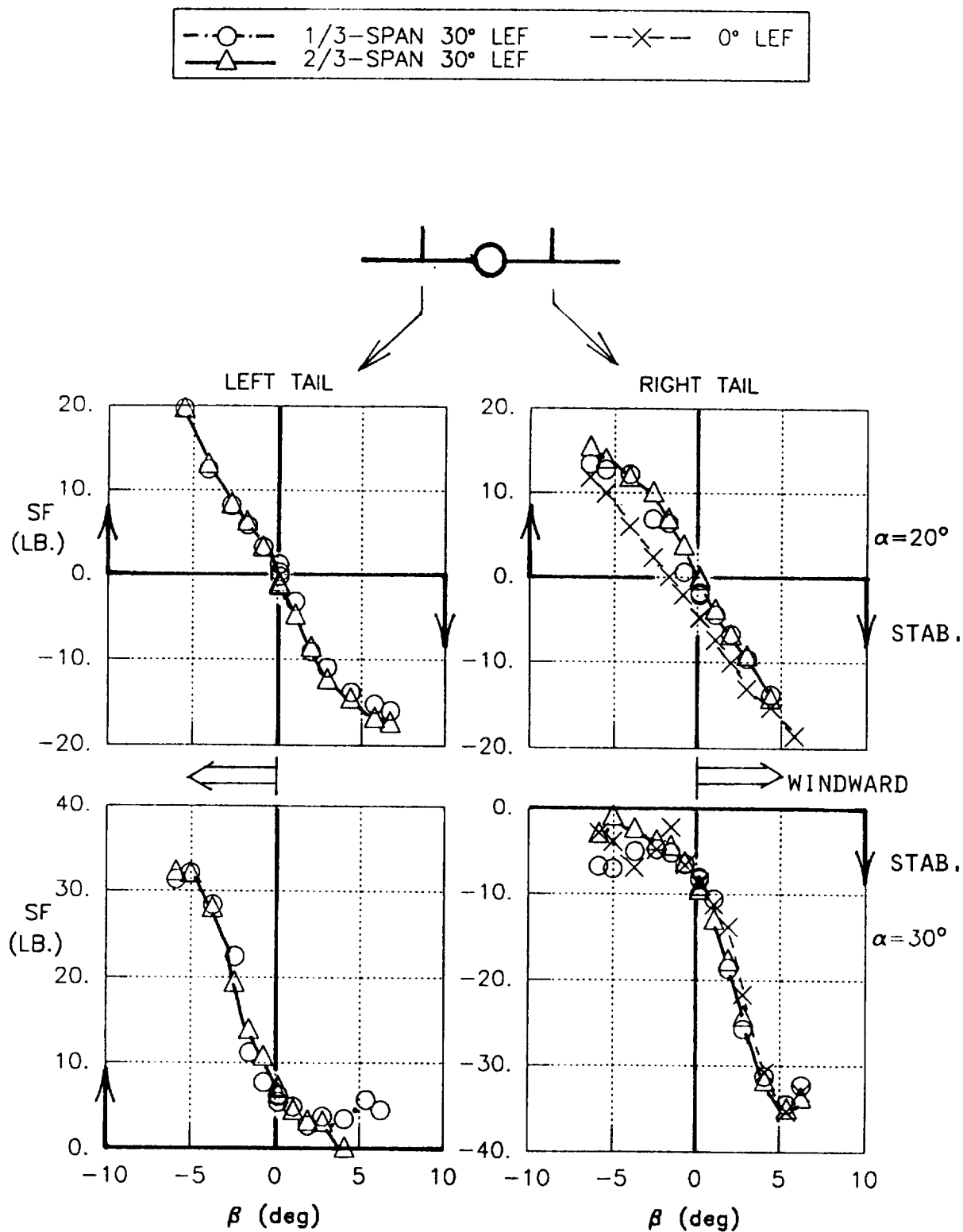Fig. 38   Twin tail static load characteristics at α = 20° and 30°, M_∞ = 0.9.

Fig. 39   Twin tail static load characteristics at α = 20° and 30°, M_{∞} = 1.2.

REPORT DOCUMENTATION PAGE

Public reporting burden for this collection of information is estimated to average 1 hour per response, including the time for reviewing instructions, searching existing data sources, gathering and maintaining the data needed, and completing and reviewing the collection of information. Send comments regarding this burden estimate or any other aspect of this collection of information, including suggestions for reducing this burden, to Washington Headquarters Services, Directorate for Information Operations and Reports, 1215 Jefferson Davis Highway, Suite 1204, Arlington, VA 22202-4302, and to the Office of Management and Budget, Paperwork Reduction Project (0704-0188), Washington, DC 20503.

1. AGENCY USE ONLY (Leave blank)	2. REPORT DATE April 1992	3. REPORT TYPE AND DATES COVERED Contractor Report

4. TITLE AND SUBTITLE
High-Alpha Vortex Decoupling Investigations on a Chine Forebody/Delta Wing Configuration at Transonic Mach Numbers

5. FUNDING NUMBERS
C NAS1-18856
WU 505-68-30-03

6. AUTHOR(S)
Dhanvada M. Rao and M. K. Bhat

7. PERFORMING ORGANIZATION NAME(S) AND ADDRESS(ES)
VIGYAN Inc.
30 Research Drive
Hampton, Virginia 23666-1325

8. PERFORMING ORGANIZATION REPORT NUMBER

9. SPONSORING/MONITORING AGENCY NAME(S) AND ADDRESS(ES)
National Aeronautics and Space Administration
Langley Research Center
Hampton, Virginia 23666-5225

10. SPONSORING/MONITORING AGENCY REPORT NUMBER
NASA CR-189642

11. SUPPLEMENTARY NOTES
NASA Langley Research Center, Technical Monitor: Robert M. Hall

12a. DISTRIBUTION/AVAILABILITY STATEMENT
Unclassified - Unlimited
Subject Category 02

12b. DISTRIBUTION CODE

13. ABSTRACT (Maximum 200 words)

This report deals with a test program conducted in the NASA Langley 8-Foot Transonic Pressure Tunnel on a blended chine/delta wing model, to verify the concept of controlled vortex decoupling via inboard leading-edge flaps for improved high-alpha lateral/directional characteristics. This test extended the Mach number range of a data base previously generated in a Langley 7- by 10-Foot High Speed Tunnel investigation. Six-component force/moment, forebody surface pressures, and central and twin tail static and dynamic loads were measured at Mach numbers of 0.4 to 1.2; laser light-sheet visualizations were also performed. Selected data are analyzed and discussed, emphasizing lateral/directional improvements and tail environment enhancement attainable by leading-edge flaps in the maximum lift region.

14. SUBJECT TERMS
High-Alpha Aerodynamics Vortex Control

15. NUMBER OF PAGES
55

16. PRICE CODE
A04

17. SECURITY CLASSIFICATION OF REPORT	18. SECURITY CLASSIFICATION OF THIS PAGE	19. SECURITY CLASSIFICATION OF ABSTRACT	20. LIMITATION OF ABSTRACT
Unclassified	Unclassified	Unclassified	